NAVAL POSTGRADUATE SCHOOL
Monterey, California

THESIS

DETERMINATION OF TIDE HEIGHTS FROM
AIRBORNE BATHYMETRIC DATA

by

Kenneth E. Welker

December 1989

Thesis Advisor: John Hannah

REPORT DOCUMENTATION PAGE

Form Approved
OMB No 0704-0188

1a REPORT SECURITY CLASSIFICATION UNCLASSIFIED	1b RESTRICTIVE MARKINGS
2a SECURITY CLASSIFICATION AUTHORITY	3 DISTRIBUTION/AVAILABILITY OF REPORT APPROVED FOR PUBLIC RELEASE; DISTRIBUTION IS UNLIMITED.
2b DECLASSIFICATION/DOWNGRADING SCHEDULE	
4 PERFORMING ORGANIZATION REPORT NUMBER(S)	5 MONITORING ORGANIZATION REPORT NUMBER(S)
6a NAME OF PERFORMING ORGANIZATION NAVAL POSTGRADUATE SCHOOL	6b OFFICE SYMBOL (If applicable) 68
7a NAME OF MONITORING ORGANIZATION NAVAL POSTGRADUATE SCHOOL	
6c ADDRESS (City, State, and ZIP Code) MONTEREY, CA 93943-5000	7b ADDRESS (City, State, and ZIP Code) MONTEREY, CA 93943-5000
8a NAME OF FUNDING/SPONSORING ORGANIZATION	8b OFFICE SYMBOL (If applicable)
9 PROCUREMENT INSTRUMENT IDENTIFICATION NUMBER	
8c ADDRESS (City, State, and ZIP Code)	10 SOURCE OF FUNDING NUMBERS

PROGRAM ELEMENT NO	PROJECT NO	TASK NO	WORK UNIT ACCESSION NO

11 TITLE (Include Security Classification)
DETERMINATION OF TIDE HEIGHTS FROM AIRBORNE BATHYMETRIC DATA

12 PERSONAL AUTHOR(S)
HELKER, KENNETH E.

13a TYPE OF REPORT	13b TIME COVERED	14 DATE OF REPORT (Year, Month, Day)	15 PAGE COUNT
MASTER'S THESIS	FROM _____ TO _____	1989, DECEMBER	107

16 SUPPLEMENTARY NOTATION THE VIEWS EXPRESSED IN THIS THESIS ARE THOSE OF THE AUTHOR AND DO NOT REFLECT THE OFFICIAL POLICY OR POSITION OF THE DEPARTMENT OF DEFENSE OR THE U.S. GOVERNMENT.

17 COSATI CODES		
FIELD	GROUP	SUB-GROUP

18 SUBJECT TERMS (Continue on reverse if necessary and identify by block number)
LIDAR, GPS, TIDE CONTROL, HYDROGRAPHY, AIRBORNE LIDAR HYDROGRAPHY, BATHYMETRY, LEAST SQUARES ADJUSTMENT, HARMONIC ANALYSIS

19 ABSTRACT (Continue on reverse if necessary and identify by block number)

Airborne Bathymetric Systems are currently under development by the U.S. Army Corps of Engineers, the Canadian Hydrographic Service, and the Royal Australian Navy. Once fully developed, the U.S. Naval Oceanographic Office (NAVOCEANO) plans to use this survey technology. NAVOCEANO faces a unique problem in utilizing airborne bathymetry, in that it plans to survey in remote and undeveloped areas of the world where tide control obtained through tide gauge deployment is often logistically and economically prohibitive. This thesis offers a method for significantly reducing the number of tide gauges needed for tide control in such a survey when the survey is conducted in an open coast environment. The approach given here provides a method for delineating a tidal zone and then suggests a

20 DISTRIBUTION/AVAILABILITY OF ABSTRACT	21 ABSTRACT SECURITY CLASSIFICATION
☒ UNCLASSIFIED/UNLIMITED ☐ SAME AS RPT ☐ DTIC USERS	UNCLASSIFIED

22a NAME OF RESPONSIBLE INDIVIDUAL	22b TELEPHONE (Include Area Code)	22c OFFICE SYMBOL
HANNAH, JOHN	(408) 646-3268	68Hn

DD Form 1473, JUN 86 Previous editions are obsolete SECURITY CLASSIFICATION OF THIS PAGE

S/N 0102-LF-014-6603 UNCLASSIFIED

Line #19 (CONT.)

survey scenario which will allow the isolation of the major components of the tidal signal through a least squares adjustment. A proof of concept simulation model developed in the thesis results in tidal depth reducers which more than satisfy IHO specifications.

Approved for public release; distribution is unlimited.

DETERMINATION OF TIDE HEIGHTS FROM AIRBORNE BATHYMETRIC DATA

by

Kenneth E. Welker
B.S., Southampton College of Long Island University, 1975

Submitted in partial fulfillment
of the requirements for the degree of

MASTER OF SCIENCE IN HYDROGRAPHIC SCIENCES

from the

NAVAL POSTGRADUATE SCHOOL
December 1989

ABSTRACT

Airborne Bathymetric Systems are currently under development by the U.S. Army Corps of Engineers, the Canadian Hydrographic Service, and the Royal Australian Navy. Once fully developed, the U.S. Naval Oceanographic Office (NAVOCEANO) plans to use this survey technology. NAVOCEANO faces a unique problem in utilizing airborne bathymetry, in that it plans to survey in remote and undeveloped areas of the world where tide control obtained through tide gauge deployment is often logistically and economically prohibitive. This thesis offers a method for significantly reducing the number of tide gauges needed for tide control in such a survey when the survey is conducted in an open coast environment. The approach given here provides a method for delineating a tidal zone and then suggests a survey scenario which will allow the isolation of the major components of the tidal signal through a least squares adjustment. A proof of concept simulation model developed in the thesis results in tidal depth reducers which more than satisfy IHO specifications.

TABLE OF CONTENTS

ACKNOWLEDGMENTS

I wish to thank all the members of the Mapping, Charting, and Geodesy Department for their help and encouragement during my time at the Naval Postgraduate School; in particular, my thanks to Kurt Schnebele who it seems is always ready to give helpful insight regarding any problem and Joseph Von Schwind for his thorough and patient teaching style. I'm grateful to Ed Thornton and Jeff Nystuen for their help and advice in the preparation of this thesis.

From outside the Naval Postgraduate School, help was forthcoming from Gary Guenther and especially Steve Gill, both of the National Ocean Service of the National Oceanic and Atmospheric Administration.

Surely it was good fortune which brought Leslie Rosenfeld to Monterey just in time to supply the missing pieces needed to complete my thesis. Her expertise in tidal theory is becoming harder to find among oceanographers and was critical in supporting the thesis.

My greatest debt is owed to John Hannah, not just for his exceptionally clear vision of adjustments and geodesy, but also for his flexibility and endless patience in assisting in the preparation of this thesis.

I also wish to mention my appreciation to my friends Joe Schild, Tim Tisch, and their families, who were a source of

encouragement as well as material support during my stay at Naval Postgraduate School.

I. INTRODUCTION

The charting of navigation routes has been important since men began using sea-going vessels for transportation. One of the first tools for measuring depths was the lead line which gave very accurate results. This device is still used, both for field calibration and where exact measures of a discrete point are desired. In this century the acoustic depth sounder was developed and is now almost exclusively used for hydrographic surveys. Until recently, the most common use of depth sounders was the single transducer depth sounder which samples the depth along the sounding line of the survey ship. However, with advances in electronic computing power has come the "swath" acoustic depth sounders. These give 100% bottom coverage by coordinating the acoustic returns of a number of transducers positioned in a wide array perpendicular to the sounding line. The result is a "map" of the bottom rather than just samples taken along the sounding line.

For an individual transducer mounted on a ship's hull, an acoustic wave travelling downward from the transducer is reflected from a point on the ocean bottom. The travel time of the signal from the transducer to the bottom and back is halved and multiplied by the estimated speed of sound through the local water column to obtain an estimate of the depth.

The latest tool for measuring depths in relatively shallow waters, (0 to 30 m), is the Light Detection and Ranging (LIDAR) survey system. It is mounted on an aircraft and operates on the same principle as an acoustic depth sounder except that the distance from the sea surface to the LIDAR platform is also measured, (see Figure 1). The chief advantage of Airborne LIDAR surveys is their speed. While a hydrographic survey vessel surveys at roughly 8 knots, an airborne survey may proceed at about 240 knots. In addition, wider coverage is obtained than in conventional surveys since the laser signal is "pulsed" at a rate on the order of hundreds of pulses per second and "scanned" perpendicular to

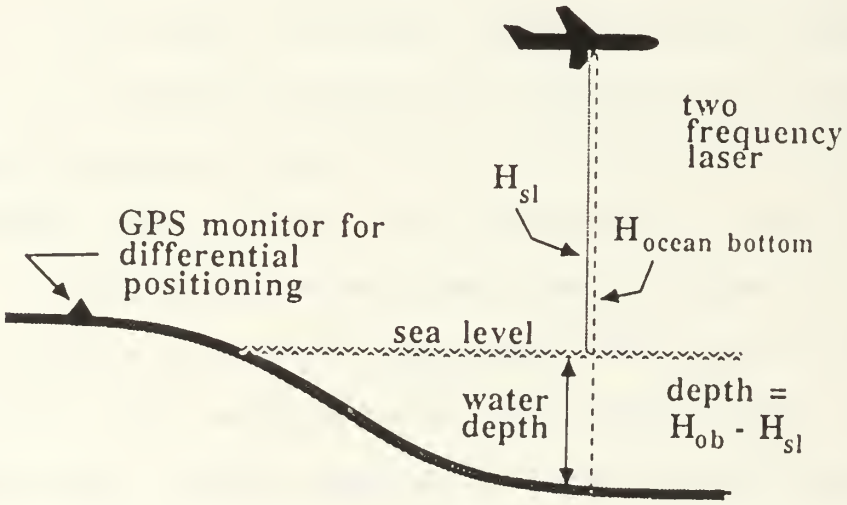

Figure 1. Laser Bathmetry. H_{SL} = Platform ht Above Sea Level, H_{ob} = Platform ht Above Ocean Bottom. (Wells and others, 1986)

the direction of flight. The combination of forward motion and scanning gives depth information between survey lines as well as along line. With 250 m line spacing 100% bottom coverage is achieved. The combined result of swath type coverage and rapid data collection rate has been estimated by the U.S. Naval Oceanographic Office (NAVOCEANO) as allowing the collection of the equivalent of 10 years of conventional ship survey data in 150 hours of airborne surveys.

Research and development of airborne LIDAR-based hydrographic systems has been underway in the U.S., Canada, and Australia for the last decade. When fully developed NAVOCEANO plans to deploy such a system.

During any hydrographic survey, tides in the survey area must be monitored in order to reduce the soundings made to a chart datum. The chart datum is a "tide based" plane which usually corresponds to some mean of the low waters for the local tidal regime. A low water plane is used so depths published on a nautical chart are shown in their least favorable aspect. If the chart datum is very conservative, corresponding for example to lowest expected tide, the depth will theoretically never be less than the published chart depth.

In a conventional open coast ship survey, monitoring the tides involves deploying at least one coastal tide gauge and perhaps a number of sea bed tide gauges. The coastal gauge should be monitored, and maintained, both during the actual

depth sounding period and also for a period of 30 days in length. Interruptions should be kept to a minimum, (preferably no more than three hours). As the survey progresses away from the reference 30 day station, the tide regime changes and secondary stations in the area of the progressed survey must be installed to reduce soundings to the local chart datum. Over a period of 30 days, the more important constituents can be separated and a good estimate of tidal planes, such as mean sea level and mean low water, can be made at the reference station. These planes are then transferred to the secondary stations to obtain the chart datum at those locations.

For airborne surveys this presents a serious obstacle. Since the aircraft covers such a large area rapidly, some method of knowing the number of different tidal regimes and accompanying chart datums within the survey area, is needed. This implies monitoring the tide simultaneously at secondary stations over larger areas than in conventional surveys. More coastal tide stations will be needed unless the "tidal zone" (i.e., the area where the tide can be considered to oscillate as a horizontal surface within the allowable error), and the amplitude of the oscillation within each zone, is known.

If at the time of flight, personnel on the ground report conditions in a designated area are not suitable for the planned survey, an alternate survey area should be available if possible. If one or more alternate survey areas are to be

available, the need for tidal control is multiplied by the number of alternate areas. Without a survey vessel in this region, separate plans must be made to deploy and maintain tide stations in each the main and alternate survey areas. Personnel requirements increase and so do safety risks.

The accuracy standards for all hydrographic surveys conducted by NAVOCEANO is specified by the International Hydrographic Organization (IHO). The standard for measuring depths is identical for measuring tide heights. Ninety percent of all measured depths in 0 to 30 m must be within 0.3 m of the true depths. Ninety percent of all measured tidal heights must be within 0.3 m of the true tide heights.

If by some method the tidal zone boundaries could be delineated, and if tidal amplitude and phase within the zones could be both predicted and verified, the number of tide gauges required could be drastically reduced. The purpose of this paper is to propose a two step method of reducing the number of tide gauges needed in an airborne LIDAR survey.

The two steps proposed are:

- estimate the spatial extent of the areas where the water level rises and falls as a horizontal surface within the allowed error and within this tidal zone
- determine tide heights from the airborne survey data and compute the amplitude coefficients for the tidal constituents in the sine-cosine series used as the mathematical model.

Chapter II is a general description of LIDAR survey systems and the operating principles and considerations of

LIDAR surveys. Chapter III cites two prior oceanographic surveys which provide evidence that many shelf regions worldwide have extensive longshore zones over which the tidal signal varies little, and offers a possible method for delineating tidal zones for ALS surveys.

Chapter IV describes the determination of the tidal amplitude coefficients using crossover measurements; the comparison of mean water levels over the time and space of the survey. This has been done for various periodic natural phenomena in the past but in only a very limited way for tides. Brown (1983), attempted it from Seasat data to obtain tidal information. Because airborne LIDAR surveys are in their infancy, actual data to substantiate the methods proposed here are unobtainable at this time. Instead a simulation is offered as an indication of the viability of this concept. Chapter V describes the crossover measurement simulation model, Chapter VI shows the results, and Chapter VII has conclusions.

II. OPERATIONAL PRINCIPLES IN AIRBORNE HYDROGRAPHIC SURVEYING

The purpose of this chapter is to briefly describe airborne laser system (ALS) surveys. The two main quantities measured in ALS surveys that are critical to development of the observation equations and simulation model are instantaneous mean water surface and the height of the aircraft above the ellipsoid. These factors are treated in more detail than the others.

A. BASIC SOUNDING PRINCIPLES

The most popular laser for bathymetry is the Neodymium Yttrium Aluminum Garnet (Nd:YAG) laser (Billard, 1986). This laser can be operated both day and night. The Nd:YAG is pulsed at 532 nm (blue-green wavelength) and doubled to 1064 nm (infrared wavelength or IR). The blue-green penetrates the water and reflects off the bottom while the infrared reflects from the surface with minimal penetration of the sea surface.

As stated earlier, for an ALS survey, the measurements are made the same way as with acoustic systems. Since the airborne platform is above the ocean surface, its altitude is determined by the IR laser. The ocean depth is the difference between surface return time and bottom return time, halved and multiplied by the estimated speed of light through the local water column;

$$\Delta T = BGRT - IRT \quad (1)$$

$$D = C/n \times \Delta T/2 \quad (2)$$

and

$$n = C/V \quad (3)$$

where

ΔT = THE DIFFERENCE IN TIME BETWEEN THE TWO RETURNS
BGRT = BLUE GREEN (BOTTOM) RETURN TIME
IRT = INFRARED (SURFACE) RETURN TIME
D = DEPTH
C = SPEED OF LIGHT IN A VACUUM
n = INDEX OF REFRACTION FOR LIGHT IN SEAWATER
V = SPEED OF LIGHT IN LOCAL MEDIUM
ΔT = TIME

n IS APPROXIMATELY 1.340 FOR SEAWATER.

Referring to Figure 2,

$$R = (H-h) \times \sec(\psi) + \text{error} \quad (4)$$

where

R = range to true surface
H = the aircraft height above sea level
h = wave height
ψ = nadir angle of diagram
error = from range measurements.

If the altitude of the aircraft above the sea level is H, it can be estimated as the average value of R cos(ψ) averaged over some number of scans, with multiple ranges measured with

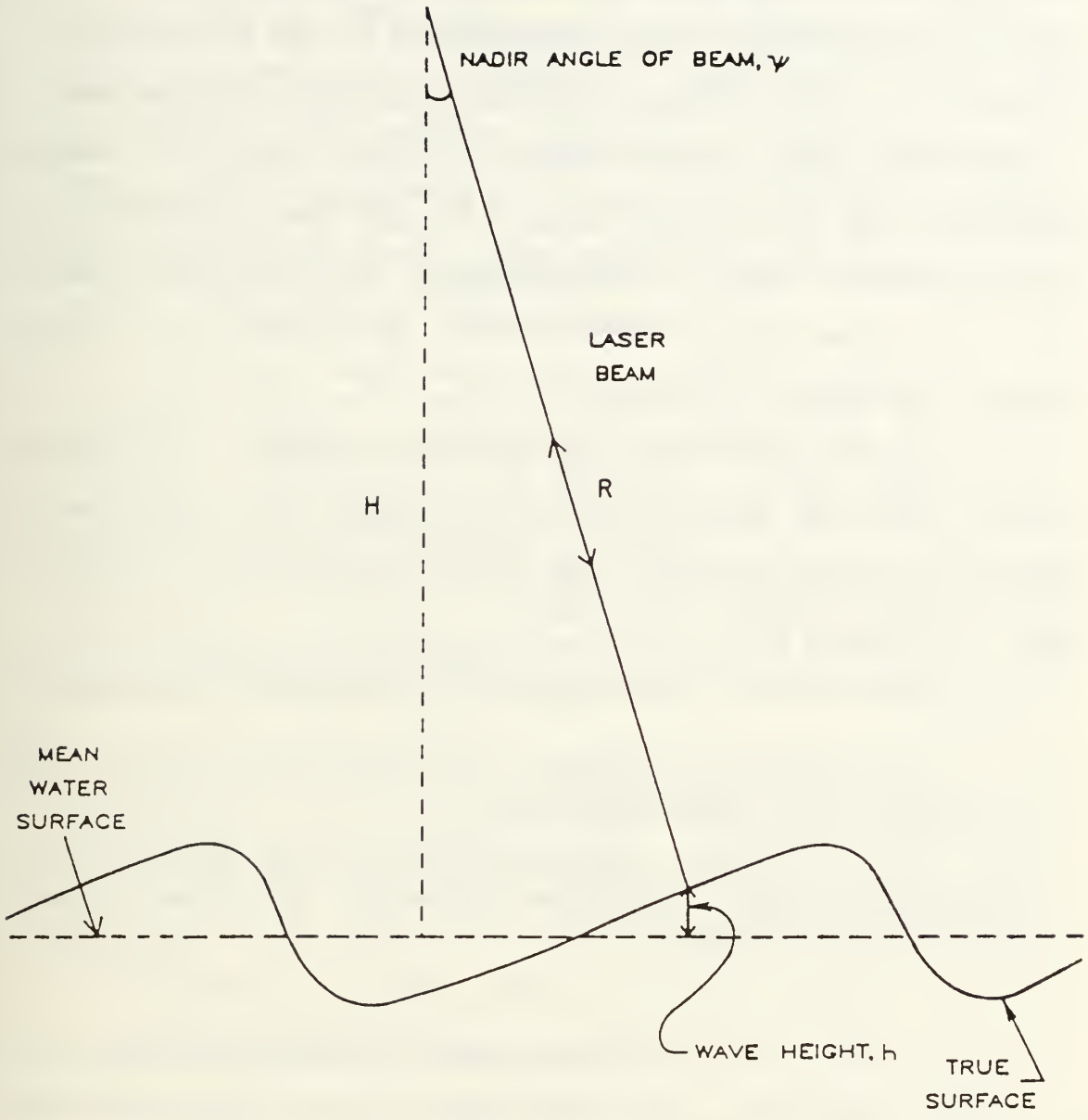

Figure 2. Wave Correction Geometry. When Nadir Angle ψ = 15°, and H = 500 m, 1/2 Total Beam Width is 134 m, "SWATH" Width is 268 m.

each scan. With H determined, it may be reintroduced in Equation 4 to obtain h from the individual ranges. Each h is used to correct the depth measurements corresponding to the individual blue-green laser measurements to the ocean bottom. The value of h is added to, (in the case of the wave trough), or subtracted from, (in the case of the wave crest), the depth measurement to refer all depths to H. It will be shown in a later paragraph that H is determined for areas that are larger than the longest wavelengths present and these wavelengths dictate the number of scans.

The ranges R may vary with vertical aircraft motion over the wave sampling area. This motion is separated into several components which describe the total aircraft orientation. These components are;

- α: angle between scanning mirror normal and its rotation axis
- β: angle between scanning mirror rotation axis and aircraft truck (downward) axis
- Γ: axial rotation of scanning mirror with θ equal to 0 degrees for port, 90 degrees forward, 180 degrees starboard, 270 degrees aft
- Pitch: pitch, aircraft pitch, positive is nose up
- Roll: roll, aircraft roll, positive is port wing up.

These components are determined in a least squares adjustment in which the ranges are used as the measured quantities. In this way R can be corrected for vertical motion.

B. METEOROLOGICAL OPERATING CONDITIONS

The following is quoted from Caviness, 1989:

> Once requirement areas have been defined, NAVOCEANO will base its decisions on when and where and how to deploy the ABS on an examination by season of historical data such as water transparency, water depth, sea state and visibility. Water transparency and depth will be used to develop "Kd" contours, where Kd is the product of K, the attenuation coefficient for diffuse downwelling light, and d, depth. Although K will usually be determined from historical data such as water quality atlases, advance tide gauge deployment teams may be able to make on-site determinations of representative values of K prior to actual deployment of the airplane.
>
> Historical data will also be used to determine the time of the year during which reasonably low winds (Beaufort Force 3 or less) and reasonably high visibility (5 km or greater) can be expected. Winds higher than Beaufort 3 can create waves of such magnitude that bottom sediments are disturbed and resuspended, thus decreasing water clarity to unacceptable levels. Large waves also result in unacceptable beam spreading caused by increased wave slope. Visibility is important not only because of airplane safety considerations, but also because of the diminished depth measurement capability which results from operation through rain or fog.
>
> Historical data will provide some indication of the likelihood of a given area being suitable for airborne hydrography at a given time. However, unforeseen circumstances like unusual storm activity or plankton blooms may destroy the validity of the predictions. NAVOCEANO will use both on-site reconnaissance and designation of secondary survey areas to overcome this problem.

C. MEAN WATER SURFACE DETERMINATION

Mean water surface (MWS) must be distinguished from mean sea level (MSL). MWS is the surface remaining after waves with wavelengths much less than the sampling area dimensions are filtered out. Referring to Figure 3, it is seen that most of the wave energy present at the high frequencies which

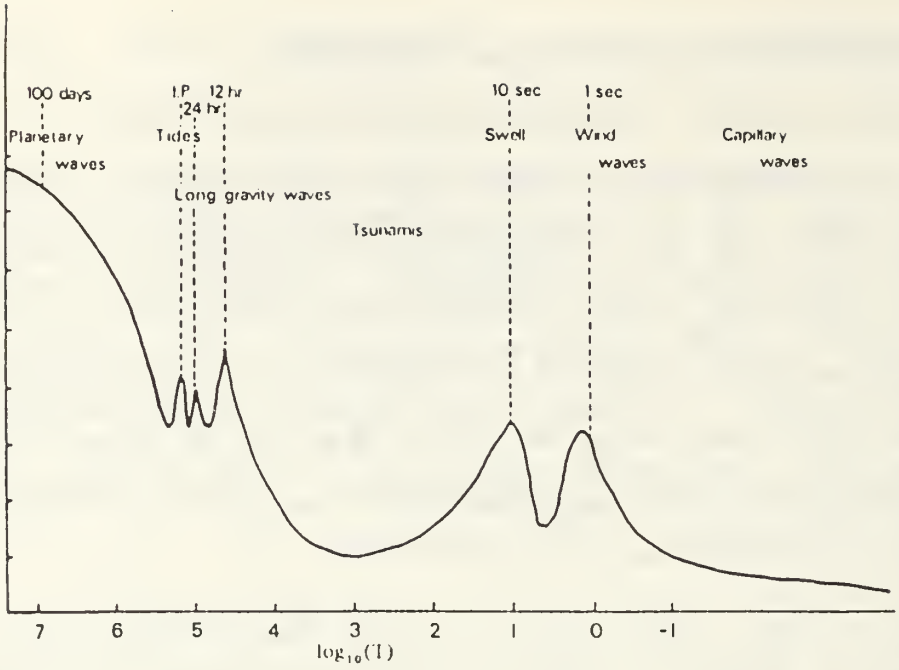

Figure 3. A Schematic Estimation of the Wave Energy Spectrum for a Mid-Latitude. (Leblond and Mysak, 1980)

obscure the instantaneous MWS (instantaneous meaning over a time scale on the order of 30 seconds), are wind generated swell or waves with periods near ten seconds. Finding a good estimate of MWS, (referred to as sea level in Figure 1), is necessary to get the true depth. The ordinate of Figure 3 is unitless since the figure is not an actual energy spectrum but just indicative of relative energy versus frequency.

On a typical ocean surface, MWS is obscured by a number of waves with period usually less than 15 seconds. This is especially true of the milder seasons when wind is diminished. The period of wind waves varies geographically and seasonally.

The objective of this thesis is to mathematically describe and measure waves of the tidal period so they can be removed from the depth measurements. Then the depths can be related to MSL or to some related chart datum. Before this is possible and before instantaneous depth measurements are possible, the higher frequency wind waves must be filtered out.

1. Capillary Waves

The highest frequency waves present are capillary waves, named for their restoring force, water surface tension. These waves are small in amplitude and have wavelengths on the order of centimeters. They are caused by wind blowing over the surface.

2. Wind Waves

With increasing period, gravity replaces surface tension as the restoring force for ocean waves. Gravity waves have larger amplitudes, periods, and wavelengths than capillary waves. Among gravity waves, wind generated gravity waves are abundant on the ocean surface (again as shown in Figure 3).

Table 1 shows properties of typical open ocean "deep water," (defined below) gravity waves. The longest period wave listed in Table 1 is 15 seconds. Such a wave would normally be encountered during the stormy winter season along the Pacific Coast of North America.

TABLE 1

PROPERTIES OF TYPICAL OCEAN WIND WAVES
(DUXBURY AND DUXBURY, 1984)

Wave Period (seconds)	Wavelength (m)	Maximum Wave Height (m)	Wave Speed (m/sec)
1	1.56	0.22	1.56
2	6.25	0.89	3.12
3	14.05	2.01	4.68
4	24.98	3.57	6.25
5	39.03	5.58	7.81
6	56.21	8.03	9.37
7	76.50	10.93	10.93
8	99.92	14.27	12.49
9	126.47	18.07	14.05
10	156.13	22.30	15.61
11	188.92	26.99	17.17
12	224.83	32.12	18.74
15	351.29	50.18	23.12

3. Filtering Out Short Capillary Wind Generated Waves

The "spot" size refers to the infrared (IR) laser beam footprint on the water surface. The return from the spot area is averaged through signal processing to give MWS over the spot, with the high frequency capillary waves filtered out. These capillary waves have wavelengths much shorter than the spot size diameter. Spot sizes vary from 2 to 25 m in diameter.

4. Filtering Out Longer Gravity Wind Generated Waves

Instantaneous MWS is determined from the average of surface returns over an area significantly larger than the largest surface waves present. This area will be as wide as the scanning width, but may vary in length by averaging for longer along track distances. In order to get a good IR

signal return from the surface, early tests have shown the maximum acceptable angle of incidence with the nadir, (ψ in Figure 2) is 15 degrees. For laser depth penetration reasons, the optimal flying height is 500 m. The tangent of 15 degrees multiplied by the flying height gives half the swath width, 134 m, or a swath width of 268 m.

The Australian prototype WRELADS scans over the sea in a rectangular pattern 260 m wide. The Laser Sounder which was a prototype tested as part of the Airborne Bathymetric System (ABS) by the Naval Ocean Research and Development Activity (NORDA) scanned in an elliptical pattern and had a 268 m width. LARSEN, the Canadian version of ALS, scans over 270 m.

5. Near Shore Waves

The following excursion into near shore linear wave approximation relates these scan widths to the feasibility for estimating MWS in the expected operating wave environment. "Deep water waves" are those that satisfy the relation,

$$D/L > 1/2$$

where

D = DEPTH
L = WAVELENGTH.

For a deep water wave the wavelength is given by,

$$L = g \times T^2 / (2 \times \pi) \qquad (5)$$

where

g = THE MAGNITUDE OF GRAVITATIONAL ACCELERATION
T = WAVE PERIOD
π = 3.14 RADIANS.

With the previously mentioned seasonal operating constraints, waves with a period greater than 15 seconds will be infrequent. For a deep water wave with T = 15 seconds, L is 351 m. Because the laser penetration depth is rarely greater than 30 m, the relation D/L > 1/2 for deep water waves will not hold in typical survey depths. Since period is unchanged, (i.e., the number of wave crests is conserved) for ocean waves, the wavelength L must change over shallower depths. As the 15 second wave makes the transition from "deep water" to shallower water, it is defined as an "intermediate" wave when;

$$1/20 < D/L < 1/2.$$

The intermediate wavelength is given by:

$$L = [(g \times T^2)/(2 \times \pi)] \times \tanh(2 \times \pi \times D/L). \quad (6)$$

In 30 m of water with T = 15, L is 235 m.

As the wave propogates to still shallower depths, it eventually meets the shallow water wave criterion. In 11.5 meters of water, our original wave now has the relation for "shallow water waves";

$$D/L < 1/20$$

and

$$L = T \times (g \times D)^{1/2} \qquad (7)$$

L is 162 m in 12 m. Thus waves with periods less than 15 seconds have wavelengths shorter than the scan width. Waves are sampled along track also. At 130 m/s flight speed, the aircraft may sample over a distance of 3900 m with 30 second averaging. With this procedure, waves which are likely to make up the ocean surface of the typical airborne survey area may be sufficiently sampled, and the MWS found by averaging. MWS may be viewed as the plane which oscillates over a longer, tidal period. At the present it is thought that the accuracy in determining MWS is 5 to 10 cm (Guenther 1989). The limiting factor in the ability to determine MWS is the precision of the laser range measurement.

D. SPATIAL EXTENT OF SURVEY

In all hydrographic surveys the survey area is delineated before the actual survey begins. In ALS surveys since the surveys are limited to 30 m in depth in most cases, and because the aircraft is capable of covering long distances rapidly, the survey "blocks" will usually be long in length (alongshore) and much less in width (offshore).

1. Sounding Lines

The most efficient way to run sounding lines in ALS surveys is parallel to shore (whereas in conventional surveys the sounding lines are run perpendicular to the bottom contours, usually this is perpendicular to shore). Since turns are very time consuming, the longer the lines the better. With this in mind a desirable survey block would have dimensions of 200 km alongshore and 1 km offshore. A survey block of this size may be surveyed in about 12 hours. P-3 aircraft can operate for 14 hours, which allows transit time to and from the survey area.

The sounding lines which run parallel to shore should be run from the shallow inshore boundary of the survey block out to deeper waters until the depth of light extinction is reached. These lines are called principal sounding lines. Since the scan width of the laser is roughly 268 m, principal sounding lines spaced 250 m apart will give roughly 18 m overlap and 100% coverage of the survey area ocean bottom. In conventional surveys a second set of lines called cross check lines are run perpendicular to the principal lines. The purpose of crosscheck lines is traditionally for checking the accuracy of the positioning system used. A depth measured at a point in the survey area should agree with the tide corrected depth measured at the same point but at a later time. If the two measured depths do not agree, it is assumed the positioning is in error. Crosscheck lines are less dense

than the principal lines and for ALS surveys will be run at ten times principal line spacing (2500 m apart).

2. Positioning with the Global Positioning System

All surveys require the horizontal position of the measured depth to be known within IHO specifications. It is anticipated that the positioning for the LIDAR platform will be by means of the Global Positioning System (GPS). GPS is capable of providing 15 - 20 m probable circular error (CEP) horizontal positioning (which satisfies the IHO specifications for 1:50,000 surveys), with a minimum of sophistication. As will be seen later, a very accurate vertical position is needed in order to enable us to extract the tidal signal from measurements (see Figure 4). The following is a superficial discussion of the operational options for GPS in order to lay the foundation for a discussion of the more precise methods of "relative" vertical positioning.

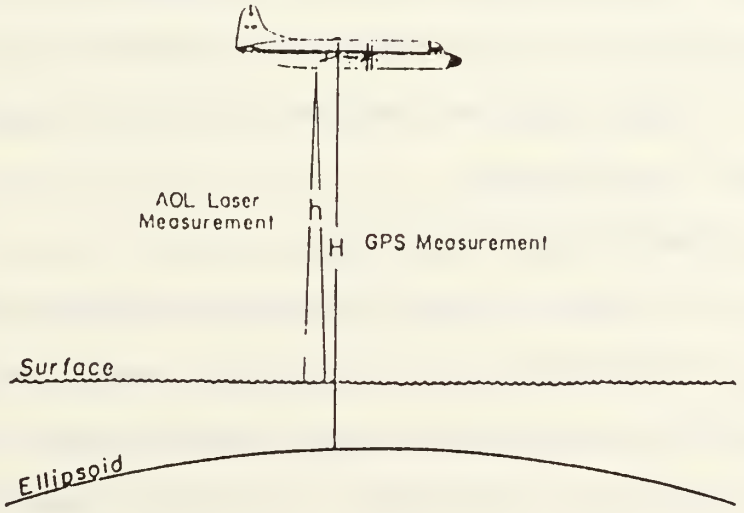

Figure 4. Mean Water Surface (MWS) Height above Ellipsoid, H-h. (Krabil and Martin, 1987)

E. AIRCRAFT POSITIONING BY GPS

The GPS will when fully implemented, consist of 21 operational satellites plus an additional three in-service spares. These satellites will be distributed in space so that at least four and as many as 10, at any instant, will be above the horizon for any observer at almost any point in the world.

Each satellite broadcasts on two L band (carrier) frequencies. The L1 frequency is broadcast at 1575.42 Mhz and the L2 frequency at 1226.60 Mhz. These carrier wave frequencies have wavelengths of approximately 19 cm and 24.4 cm respectively. In addition, each satellite broadcasts two codes, C/A and P, each with the appearance of psuedo-random noise, which are modulated onto the carrier frequencies. The L1 carrier is modulated with both codes while the L2 carrier will generally have P code modulation only. The C/A code, known as Coarse Acquisition code, has a wavelength of 300 m while the P (Precision) code has a wavelength of 30 m. Most GPS receivers have the ability to interpolate the received phases (whether they be carrier or code) to approximately 1 % of their wavelengths.

1. Psuedorange Positioning

This type of positioning (sometimes called absolute or point positioning) can be done in real time and requires equipment at the least level of sophistication. In principle, the GPS receiver generates a C/A code identical to that modulated onto the L1 carrier received from the satellites.

The C/A code, as received from the satellite, is correlated with an identical code generated by the receiver and the time delay required for the signal to travel from the satellite to the receiver, determined. If the satellite and the receiver clock oscillators were exactly synchronized, the time delay, when multiplied by the speed of light (c) and corrected for atmospheric delays, would represent an exact measure of the range from the receiver to the satellite. Since such synchronization is difficult to achieve, a clock offset unknown is introduced into the range equation which is given by:

$$\text{Range} = ((X_s - X)^2 + (Y_s - Y)^2 + (Z_s - Z)^2)^{1/2} + c\,\Delta\tau \qquad (8)$$

where X, Y, Z (the receiver position) and clock offset, ($\Delta\tau$) are the unknowns. We assume here that the position of the satellite in three dimensional space, (X_s Y_s Z_s), at any instant, is known. Thus if we have as a minimum, at least four satellites in view, we are able to generate four simultaneous equations and solve for the unknowns.

It is anticipated that a C/A code solution, once the GPS system is fully operational, will have an accuracy of approximately 100m CEP. However, authorized users, which will include U.S. government agencies, should be able to access the more precise P-code which in turn is expected to produce the 15-20m CEP horizontal positions required for the bathymetric surveys described here.

2. Carrier Phase Positioning

As we indicated earlier, a much more precise vertical position (or rather vertical position difference) is required to support the tidal recovery technique which will be outlined later in this thesis. The means by which these very accurate relative position differences may be obtained is now described.

Relative positioning can occur when two (or more) stations simultaneously track the same satellites. Under certain conditions, the relative positions between these stations can be determined with a great deal of accuracy. In practice, when two stations track two (or more) satellites simultaneously and record the carrier phases on both the L1 and L2 frequencies, it is possible to set up phase difference observation equations from which many of the error sources inherent in point positioning are eliminated. For example, the effects of satellite and receiver clock instabilities are largely eliminated as are the effects of any errors in the satellite ephemerides. In addition, the differencing procedure, at least for stations up to 200 km apart, will help eliminate unmodelled tropospheric delay error in the received signals. The use of dual frequency equipment is vital in the application being considered here since two frequencies are the minimum required in order to give a first order estimate of the ionospheric delay error, a delay which, at the present

time of high sunspot activity, can account for residual range errors in the order of meters.

The primary disadvantage of carrier phase differencing hinges around the need to resolve the integer phase ambiguities inherent in the measurement. Recall now that the wavelengths of the carrier waves are either 19 cm or 24 cm and that our equipment (under this technique) can only resolve the phase in the last wave. It should be clear that there will be an unknown but integer number of waves between the receiver and the satellite. A number of techniques are available for resolving this integer ambiguity when, as in our case one station is fixed (i.e., on the ground) and the other is moving (i.e., attached to the aircraft). These techniques are described in Mader and Lucas (1988) and Kleusberg and others (1986) and generally require an approximate collocation of receivers prior to the survey.

In practice, as with the absolute positioning technique described earlier, it is necessary for the ground station and the receiver on the aircraft to observe at least four common satellites throughout the survey period. In addition, at least one ground receiver and the receiver on the aircraft should have their integer ambiguities resolved prior to the survey. For the application under consideration here, it is suggested that at least three dual frequency receivers be deployed, one on the aircraft, one at the airport on a fixed station (to facilitate integer ambiguity resolution) and

one at the tide gauge near to or adjacent to the survey region. This latter receiver will provide the reference tracking station for the survey.

3. Accuracy Now Available

Krabil and Martin (1987) give relative positioning test results using the phase measurement method which show a 12 cm one standard deviation in relative vertical positioning even with poor satellite geometry. During this test one of the four satellites being observed had an elevation angle of about 20 degrees. This was the only satellite which could not be tracked continuously on both the L1 and L2 frequencies. The receivers used during the test were capable of tracking only four satellites at a time.

New receivers are now available which can track up to 12 satellites at once. When a full constellation of GPS satellites is in place, it seems likely that at least four satellites will be able to be tracked continuously on both the L1 and L2 for the entire length of an airborne survey (see Figure 5).

The problems of ionospheric correction, and some of those associated with the phase ambiguities may be overcome if the requisite number of satellites are tracked on both frequencies throughout the flight. More experience is needed in tracking GPS satellites in the kinematic mode to know the best accuracies which may be obtained. Krabil and Martin (1987) speculate 1 - 2 cm relative vertical positioning with

good satellite geometry. This is more than adequate for measuring instantaneous MWS in reference to the ellipsoid. The vertical positioning error used in the simulation described in Chapter V is 5 cm.

It will be shown in a later section that the combination of 10 cm accuracy in measuring MWS in relation to the aircraft and 5 cm accuracy in relating the aircraft to the ellipsoid is the equivalent of measuring the MWS on a tide staff to the combined accuracy $(5^2 + 10^2)^{(1/2)}$ and the difference in the two measurements is $(2)^{1/2}$ times the single measurement accuracy.

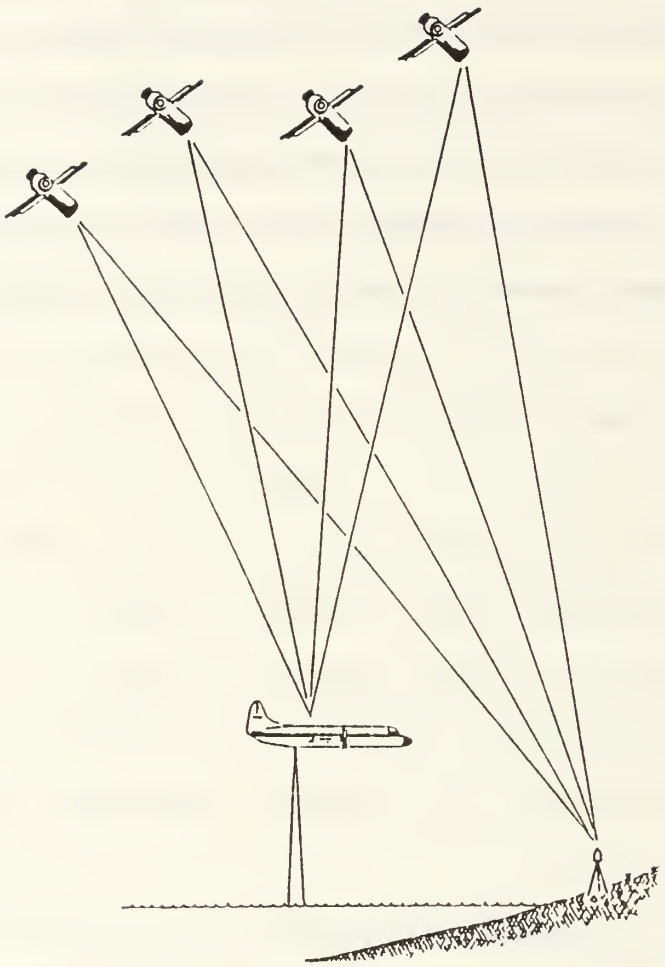

Figure 5. Differential GPS Kinematic Positioning, (with Full Constellation). (Krabil and Martin, 1987)

III. THE TIDAL ZONE

A. INTRODUCTION

The purpose of monitoring tides during a hydrographic survey was briefly discussed in the introduction. The tidal zone defined there is the subject of this chapter. The approach offered in this thesis for minimizing the number of tide gauges deployed during an ALS survey is restricted in application to the open coast. This is so since only along the coasts of large ocean basins does the tidal zone, as defined in the introduction, extend for distances greater than the length of a typical ALS survey area, say 200 km. In smaller basins (e.g., gulfs, seas, bays, estuaries, rivers), the tidal zone may change over distances on the order of a mile. Where the tidal zone changes rapidly, tide gauges must be deployed in each zone to obtain the local tidal sounding reduction.

The purpose of this chapter is two fold; first to substantiate the fact that along the open coast the tidal zone extends for long distances; and secondly to show that the tidal zone extends seaward much further than the typical continental shelf survey area. The method used to illustrate that the tide has an unchanging amplitude across the shelf may also be used as a survey planning tool which divides the shelf region of interest into survey blocks or tidal zones. In

addition to coastal tide gauge records, several oceanographic studies support the contention that coastal tides can be similar for distances on the order of 2000 km. Two such studies are discussed here.

A further qualification is required regarding the two studies cited here; both deal only with barotropic waves. In barotropic motions the surfaces of constant density, (isopycnals), remain parallel to each other and to the surfaces of constant pressure, (isobars). The isobaric surfaces and isopycnal surfaces oscillate in phase. In a fluid where there is vertical stratification of density, baroclinic as well as barotropic motions can occur. In baroclinic motions, the phase of isopycnal oscillations may vary with depth, and so do not remain parallel to each other or to the surface formed by the air water interface, often referred to as the "free surface." Internal waves, which can exist at tidal frequencies, are baroclinic motions. The amplitude of the free surface displacement due to tidal period internal waves is only on the order of a centimeter. In the tide height determination procedure proposed in the next chapter, the contribution of internal waves to the surface displacement is not treated separately since it is so small. Also, over the short time period of an ALS survey, the internal and surface tides are likely to be phase-locked. The surface signature of all waves of tidal frequency is modelled.

B. THE EXTENT OF THE TIDAL ZONE

1. The Length of Waves that Cause the Tide

The major components contributing to the rise and fall of the tide occur close to diurnal (12 hour) or semidiurnal (24 hour) period. The oscillation of the water surface on the ocean is caused by very long waves which are primarily forced by the moon and sun at these tidal frequencies. The tides are larger in amplitude in the oceans, and the basins with access to the ocean, than in land locked bodies of water. This occurs because only the oceanic sized basins can accommodate waves of planetary scale, such as the waves which occur as a response to tidal forcing. Kelvin waves created by tidal forcing rotate around an amphidromic point where the water level does not oscillate due to tidal forcing. As the distance from the amphidrome increases, the amplitude of the wave increases. The amphidromes in the ocean basins have been approximately located. The interaction of the tide wave with the shelf topography is exceedingly complex.

Munk and others (1970) have modelled the Kelvin like progression of both semi-diurnal and diurnal tide waves along the California coast. They show the variation of sea level due to tides along the coast as a linear superposition of three wave approximations;

- Kelvin (mode zero coastally trapped wave)
- Poincaré-like leaky wave and
- a forced wave (the distortion of the sea floor by tide producing forces plays a significant role).

These are solutions to the equations of wave motion that satisfy the boundary conditions "for waves along an infinitely long straight shelf in a rotating system, with the opposite coast infinitely distant," in other words along a continental shelf. The solution they arrived at was dependent on the local inertial period 2 π/f, where f, the coriolis parameter, equals 2Ωsin(ϕ), where Ω is the speed of angular rotation for the earth, and ϕ is the latitude which is taken as constant for the spatial extent of the solution. The waves were modelled as;

$$\eta(y,t) = \sum_j [a_j \cos(\beta_j y - \omega t) + b_j \sin(\beta_j y - \omega t)] \qquad (9)$$

where

η = sea level above the still water level
y = the alongshore axis
j = number of wave components
a_j = amplitude coefficient of the jth cos term
β_j = the longshore wavenumber of the jth component wave
b_j = amplitude coefficient of the jth sin term
ω = the frequency of the tidal constituent.

In terms of the traditional representation of sea level at some time t and related to some chosen tide station, y = 0,

$$\eta(y,t) = h(y) \cos[\omega t - g(y)] \qquad (10)$$

where h(y) and g(y) are the tidal constants of amplitude and phase at tide station y. This gives the relations:

$$h \cos g = \sum_j [a_j \cos \beta_j y + b_j \sin \beta_j y] \qquad (11)$$

and

$$h \sin g = \sum_j [a_j \sin \beta_j y - b_j \cos \beta_j y] \qquad (12)$$

A least squares fit of amplitude coefficients to coastal and offshore tide measurements gives a multi-component wave model which closely imitates the real progression of the tide wave along the coast of California. The model can predict the expected tides for the coast from La Jolla to Crescent City with only minor anomalies, see Figure 6. Heavy, smooth curves refer to the theoretical model developed above. The anomalies found in this study are a non-uniform wave propagation rate along the northern part of the coast. The authors speculate that this lag may be due to perforations in the boundary in the form of the bays in the northern part of the coast. These perforations are believed to act as capacitors, which interfere with the alongshore propagation of the wave by absorbing some of the wave energy and emitting some energy stored in the harbor at a subfrequency. The reason for noting this here is that if sections of coastline are to be partitioned as areas of likely uniform tide, such perforations should be treated as either boundaries or areas where tide measurements are required. Munk et al., show that before the perforation there is no interference, whereas afterwards there is. They note that this effect falls off as the wave propagates away from the perforation in proportion to 1/k, where k is the open ocean wave number. In the next section

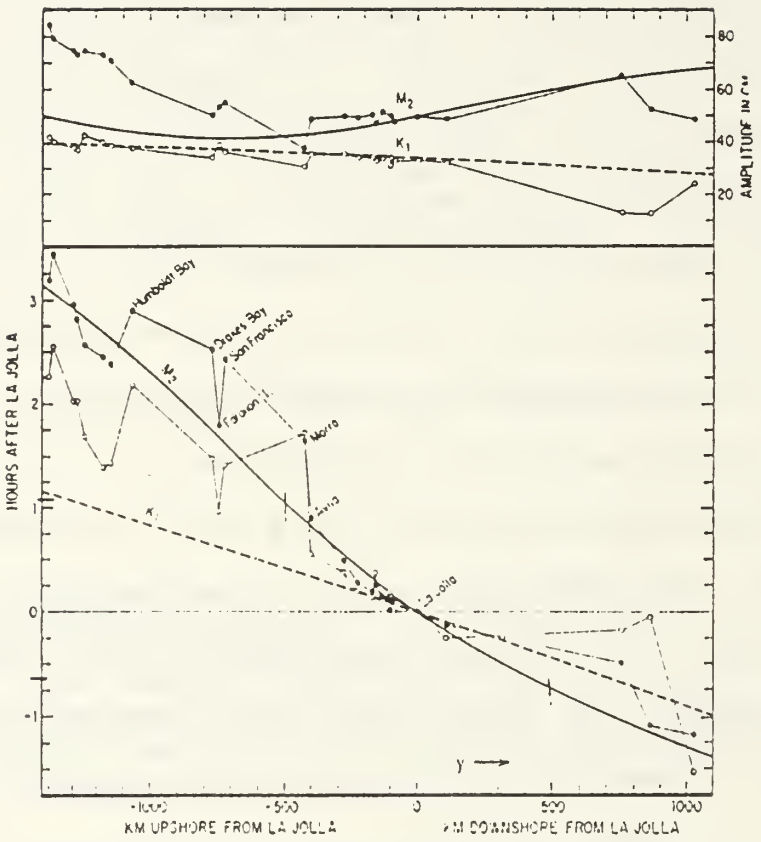

Figure 6. Amplitude and Phase Anomalies Due to Irregular Coastline. The Upper Panel Gives the Variation in Amplitude Along Shore, the Lower Panel the Corresponding Variation in Phase. Solid Circles and Solid Lines Refer to the Lunar Semidiurnal (M_2) Constituent; Open Circles and Dashed Lines to the Lunarsolar Diurnal (K_1) Constituent. (Munk and others, 1970)

it will be shown that in the absence of alongshore irregularities such as perforations in the boundary or bends in the coastline, the tidal zones can be characterized by partitioning off sections of similar shelf width and estimating the magnitude of the amplification across this shelf. If the amplitude of the tidal constituents were known seaward of the shelfbreak, the amplitude near the shore might be estimated. To use the amplification factor to partition the shelf into tidal zones in preparation for an ALS survey, information about the amplitude of the deep ocean tides may be obtained from models.

Global tide models have been developed which agree with observed tides with differing accuracies depending on region. The greatest weakness in tide models is in predicting the tide near the shore. This is due to the non-uniform shape of adjacent shore sections which interact differently with the same wave. This problem may be overcome by making observations of the tide in the tidal zone of interest. Such observations are the subject of Chapter IV.

Munk and others, found that the shortest component wave of the M_2 frequency composite was the Kelvin wave which was 8000 km long. This suggests the extent of this semi-diurnal tidal regime. The diurnal tide waves are longer still. By developing the wave type solutions possible in an ocean basin, and showing that a superposition of these waves in a model can account for the tides over an extensive alongshore

distance, Munk and others, have built a theoretical foundation for the proposition that tides are similar for long distances along the open coasts of large oceanic basins.

C. TIDAL AMPLIFICATION ACROSS THE SHELF

A suggested method for partitioning these extensive alongshore distances into tidal zones is the remaining subject of this chapter. Referring to Figure 6, it is seen that both the amplitude and even more so the phase, have abrupt changes over the alongshore length of the tidal regime. But there are sections of coast for which there are only small changes in phase and amplitude. For ALS surveys it may suffice to examine existing nautical charts and partition off sections of similar shelf width and curvature to be treated as separate tide zones. Clarke and Battisti (1981) have developed an easy method for estimating tide height amplification over "smooth continental shelves." They define smooth continental shelves as those where longshore variations in topography are on a much larger scale than offshore variations and where bends in the coastline occur on a scale much larger than the shelf width. The method of Clarke and Battisti shows both that the tide is not much different for long distances offshore and provides a means of identifying sections of continental shelf over which the tide should be similar (i.e., the "tidal zone" as defined in the introduction). That which follows is a restatement of their results with regard to amplification of

the tide wave across the continental shelf of a smooth coast. The amplification factor for the simple geometry of Figure 7 and where j goes to 2 is

$$\frac{\eta(x)}{\eta(0)} = \left[\sum_{n=0}^{\infty} \frac{(-\mu_1 a)^n}{(n!)^2} \left[1 - \frac{if'(x-a)}{\omega} + \frac{n\alpha_1}{\alpha_2} \left(\frac{x-a}{a} + \ln\left\{ \frac{h(x)}{h(a)} \right\} \right) \right] \right] \tag{13}$$

where

$\eta(x)$ = the sea level above the still water level
h(x) = depth at distance x offshore,

$$h(x) = \alpha_j (x - \beta_j) \tag{14}$$

where

$$\beta_j = \begin{bmatrix} 0 & j = 1 \\ \left[a_{j-1} - \sum_{i=1}^{j-1} \frac{\alpha_i}{\alpha_j} (a_i - a_{i-1}) \right] & j = 2, 3 \ldots n \end{bmatrix} \tag{15}$$

a = distance offshore to the continental shelf/break
l = $il(x,y)$

$$= \frac{\partial \eta}{\partial x} \quad \eta^{-1} \tag{16}$$

$$\mu_j = \frac{\omega^2 - f^2}{g\alpha_j} + \frac{if'}{\omega} \tag{17}$$

f = coriolis parameter
α_j = the slope of the jth surface, (i.e., for the continental shelf j=1, the slope, j=2)
ω = angular frequency of the tide.

When $il(x,y)$ is zero, and ν is defined by

$$\nu = \frac{\omega^2 - f^2}{g\alpha_j} a \tag{18}$$

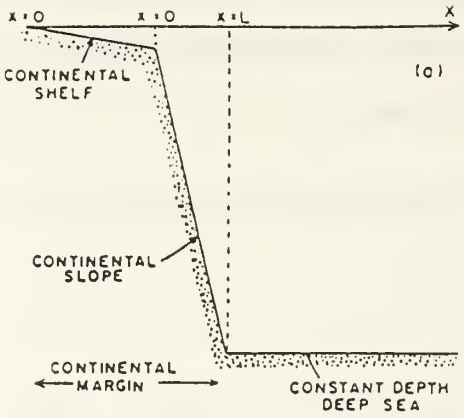

Figure 7. Geometry of Simplistic 2-Slope Continental Margin. (Clarke and Battisti, 1981)

the following plot (Figure 8) shows the behavior of the amplification factor as ν increases from -1.0.

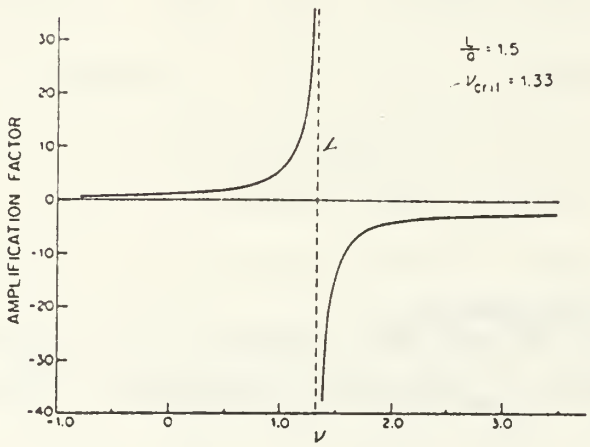

Figure 8. Amplification Factor Plotted versus ν. This Plot is for Realistic Parameters (h(a) = 200 m, h(L) = 4 km, L/a = 1.5, α_1/α_2 = 0.026). (Clarke and Battisti, 1981)

The plot shows that when ν is negative, the amplification factor is <1. This indicates that amplification will not occur for l=0 and $\omega^2 < f^2$. For latitudes from 30 degrees to the pole, ν is negative for the diurnal frequency because ω is less than f; but even at latitudes below 30 degrees at the diurnal tidal frequency ν should be small for realistic continental slopes and widths. The plot also shows that for $\omega^2 > f^2$, which is true for the semi-diurnal tide, there is amplification which starts roughly at one and grows exponentially until resonance occurs, (i.e., at ν critical). Only at the pole does ω equal f and ν is zero. ν increases primarily due to the shelf widening (i.e., large a), and remaining shallow (i.e., h(x) small).

Because

$$\frac{1}{\alpha_j} = \frac{a}{h(x)} \tag{19}$$

it follows that

$$\nu = \frac{\omega^2 - f^2}{h(x)g} a^2 \quad . \tag{20}$$

It is more apparent in this form that ν is largest for large "a," (wide shelves), and small h(x), shallow depths.

When the natural cross-shelf scale approximates the width of the shelf,

$$a = g \frac{\alpha_j}{\omega^2 - f^2} \tag{21}$$

and resonance occurs, (i.e., ν is approximately one).

The value of the function $i\ell(x,y)$ is estimated from the results of coastal tidal records alongshore. The amplitude and phases resulting from a harmonic analysis of such records are plotted in Figure 9. The noisy shape of the plot is due to the unsmooth shape of the coastal features in the vicinity of the tide gauge. By using the least squares method, a polynomial is used to smooth this plot. In Clarke and Battisti (1981), $i\ell(x,y)$ is shown to be independent of x. Thus it is possible to estimate the value of $i\ell(x,y)$ from the smoothed plot of coastal data, as shown in Figure 9.

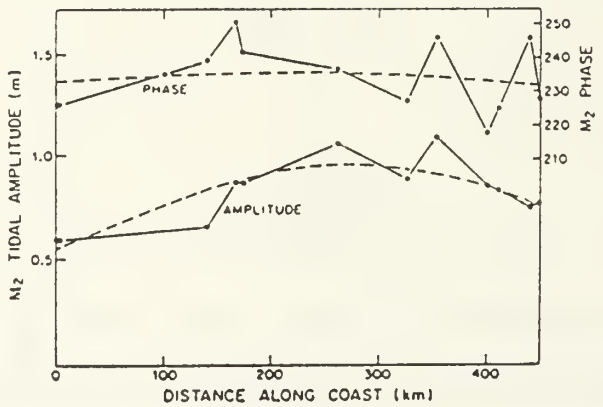

Figure 9. $i\ell(x,y)$ Polynomial Smoothing. Solid Line Shows Measured Alongshore Changes in Phase and Amplitude. Dashed Line Shows Smoothed Plot Via Least Squares Fit Polynomial. (Clarke and Battisti, 1981)

For ALS surveys the amplitude factor can be a valuable tool in predicting the length of a survey block where the tide may be viewed as a horizontal surface oscillating at the tidal frequency. Such a zone might require that the maximum difference between the tide heights at one boundary and the simultaneous heights at the other boundary must be within 0.3 of a meter of each other 90% of the time. As is shown in the Chapter IV, observations taken throughout the survey area should give a least squares fit that describes the oscillation somewhere near the center of the survey area best; but if the curve derived were to describe the oscillation at just one of the boundaries, it would still give tide heights accurate enough to reduce soundings throughout the survey area all the way to the opposite boundary. This criterion would give an initial indication of the amplitude of oscillation throughout the survey area.

The estimation of $il(x,y)$ from tide gauges has allowed Clarke and Battisti to use an amplification factor to show how the tide wave is amplified across the shelf of a smooth coast. In applying the amplification factor in ALS surveys the alongshore wavenumber, $il(x,y)$, cannot be estimated from tide gauge measurements, but could perhaps be estimated by examining the shelf structure from existing bathymetric charts and combining this information with models that give accurate predictions of amplitude and phase offshore. Since the

amplification factor is derived for, and applicable only to "smooth shelves," the function $i\eta(x,y)$ will be small along the open coast. If η were simply set to zero, the error would be small, as shown in the Clarke and Battisti paper.

The use of this method for estimating the amplification of the tide wave over the shelf of smooth coasts has been shown to be possible where $i\eta(x,y)$ can not be estimated and so is set to zero. The amplitude ratio is largely dependent on the $(\omega^2 - f^2)/(g\ \alpha)$ term while the $f\eta/\omega$ term gives the phase ratio. Clarke and Battisti apply the amplification factor in South Australia where an amplitude ratio was obtained with $i\eta(x,y)$ set to zero because it could not be estimated from coastal tide measurements. This amplitude ratio agreed well with one obtained from measurements.

Unfortunately, this thesis does not attempt to estimate the value of $i\eta(x,y)$ from a combination of model and bathymetric information. To test the validity of this approach, the estimation of $i\eta(x,y)$ should be made in an area where $i\eta(x,y)$ is known. The estimation of $i\eta(x,y)$ from offshore values of amplitude and phase obtained from models ought to be the subject of future work.

With $i\eta(x,y)$ set to zero, Figure 10 shows how the amplification factor varies for the first 1.5 km offshore (i.e., to the 30 m isobath) for a typical shelf where;

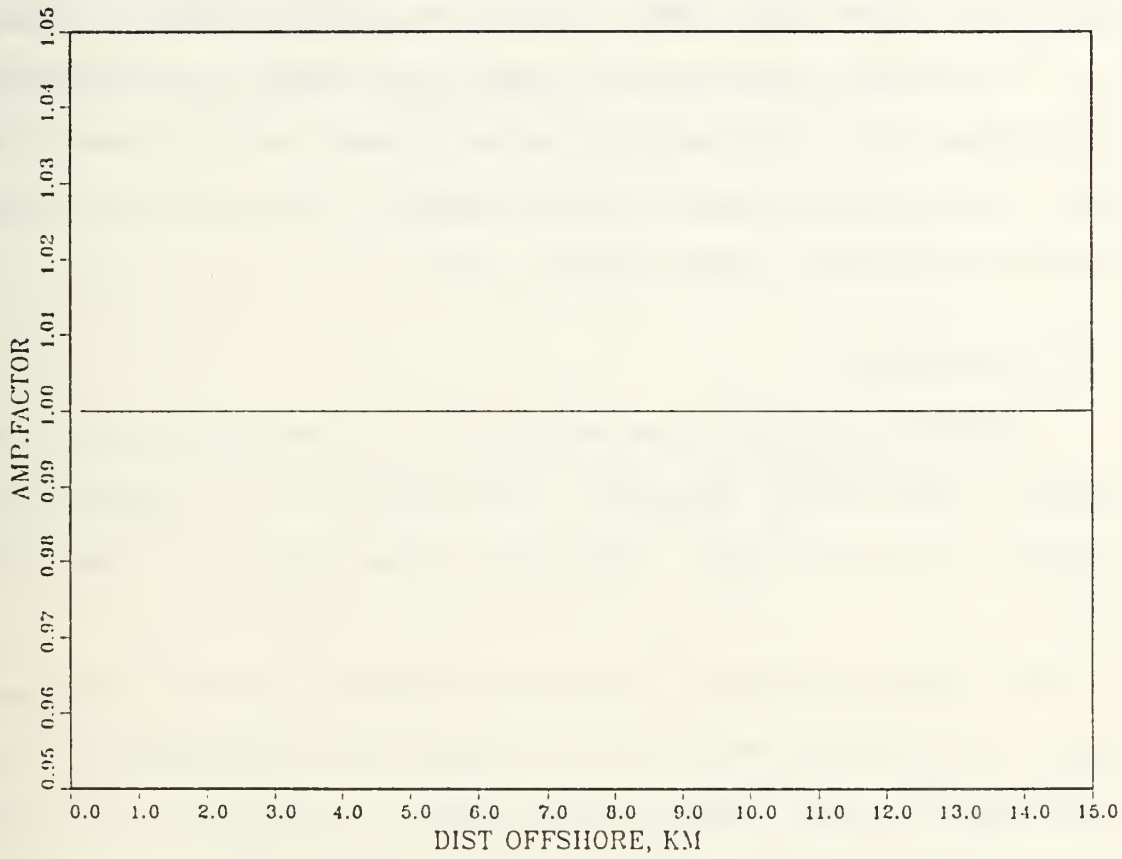

Figure 10. Amplification Over Shelf. Plot shows Amplification is Very Close to One for 15 km Offshore When $i\eta(x,y)$ is Set to Zero Across a Typical Shelf of 2-Slope Geometry as in Figure 7.

- α_1, (shelf slope) = 2 m per km
- α_2, (slope of continental slope) = 70 m per km
- latitude = 30 degrees
- shelf break = 100 km occurring at the 200 m isobath.

The line is horizontal on a similar plot which extends all the way to the shelfbreak at 100 km. As is shown in Figure 8, ν critical occurs only where the shelf is very wide. Otherwise the amplification factor is not very different from one. For the shelf used in this example, the width would have to be 1200 km for resonance to occur.

D. CONCLUSION

From the forgoing discussion, it is concluded, that along smooth continental shelves, a survey block of approximate length 200 km is small compared to the length of the tidal zone.

It follows from the Clarke and Battisti study cited here that it should be sufficient to examine the topography of the designated survey area and partition off sections of similar shelf width and curvature to be treated as separate tide zones. If these areas meet the qualitative requirement given by Clarke and Battisti for smooth continental shelves, the value of $il(x,y)$ will be small since the tide producing waves have very long alongshore wavelengths, (i.e., Order 1000 km). Where the slopes of the continental shelf and slope can be characterized, the amplification of the deep sea tidal

amplitude over the continental margin can be estimated with $i\eta(x,y)$ set to zero. These sections of shelf can be treated as tidal zones and observations throughout these zones will give a direct measure of the oscillation occurring there. It will be shown later that for the coast of California an area larger than a typical survey area meets the criterion described above for oscillation at the boundaries.

IV. THE OBSERVATIONS

A. INTRODUCTION

With the understanding that the tidal zone can extend for distances at least as long and wide as a survey area, and that the tide oscillates uniformly throughout within an acceptable error for hydrographic surveys, the next step is to isolate the oscillation of MWS caused by tidal forcing from any other oscillation. Determining how the surface of the tidal zone changes over the time and space of an ALS survey is the subject of this chapter. The method proposed here to enable the separation of the tidal variation from other phenomena is that of the crossover measurement technique, the description of which is the subject of this chapter.

B. THE COMPONENTS

The components which make up the vertical distance from the ellipsoid to the instantaneous MWS are shown in Figure 11).

The equation which represents the height of the MWS above the ellipsoid is;

$$\eta = H-h = G + SST + TS + \sigma_T \qquad (22)$$

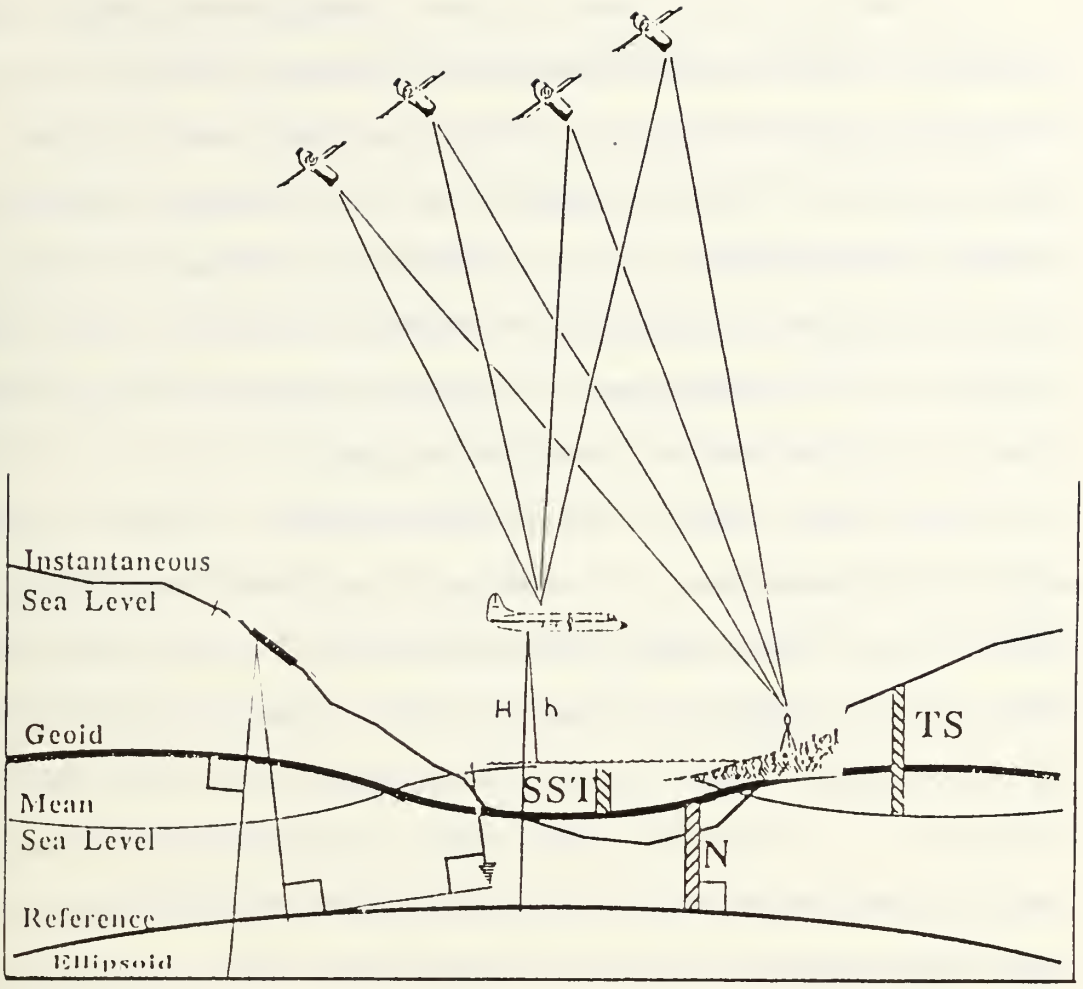

Figure 11. Components of η; Shows Components Which Comprise MWS Separation Ellipsoid Surface. (Wells and others, 1986)

where

η = instantaneous sea level above the ellipsoid
H = aircraft altitude above the ellipsoid (determined by GPS)
h = laser determined altitude of aircraft above MWS
G = geoidal undulation
SST = sea surface topography
TS = tidal signal
σ_T = total measurement error.

If the tidal zone were a plane, every measurement made of η within the tidal zone could be compared without regard to location within the zone to find the tidal oscillation. But because some of the components of η vary significantly over space, the measure of η over time must be made at the same point in space. Since cross lines are run in ALS surveys anyway, it is convenient to use the intersection of these lines as the crossover measurement point.

The first step in the development of the crossover measurement approach to isolating the tidal variation is to examine the time varying components of η. The time scale of the survey is between six and 12 hours, and the spatial scale is not greater than 200 km alongshore and up to 10 km offshore. It will be shown that the effects of the space varying components of η will be eliminated by differencing the MWS measurements at the intersection of the cross and principal lines. If the sea surface did not vary over the extent of the survey area the crossover technique would not be needed since any change in η would be due totally to tidal oscillation, (i.e., the survey area and tidal zone would oscillate as a block). But the crossover approach is needed since the amount of slope in the sea surface possible due to SST and geoidal undulation is much larger than the range of tides and may mask the oscillation due to the tide alone.

1. The Tide Signal

The tide signal is the oscillation we wish to isolate. The period of variation for TS is well known and will be discussed in a later section of this chapter. Its oscillation in vertical space, however, (i.e., the amplitude of oscillation) must be measured for a particular tidal zone and the variation in amplitude of the oscillation in horizontal space must be small from one boundary of the tidal zone to the other. In theory the open coastal tide zone oscillates with approximate uniformity throughout, the approximation falling within the error allowed by the IHO specifications for measured tide heights. The results of an application of this theory presented in a later chapter supports this proposition.

2. Sea Surface Topography

Sea surface topography varies in both space and time. There are two causes for SST; they are the quasi-permanent component which changes immeasurably over survey time scales, and a transient component which may have a measurable effect on SST even over survey time scales, but will be shown to be small in a typical ALS survey situation.

The quasi-permanent component is caused by geostrophic ocean flow which deforms the sea surface in phenomena such as westward intensification (e.g., the Gulf Stream) and smaller scale geostrophic features such as rings and gyres. The location of this type of surface distortion varies slowly over survey time scales and the depth reached by these phenomena

limit their presence to the deeper ocean seaward of the continental margin, beyond the depths where ALS surveys are conducted.

The transient component of SST is related to meteorological conditions. These include wind driven water build-up both away from and against the shore, (commonly called set-down and set-up respectively), river discharge, and the inverse barometer effect. In severe storm situations meteorological causes of SST can change η on the order of meters over survey time scales. But given the seasonal and daily constraints discussed in Chapter I regarding ALS operating conditions, the change is SST over survey time scales should be small. Referring to Figure 12, it is seen that if ALS surveys are conducted during seasons of moderate

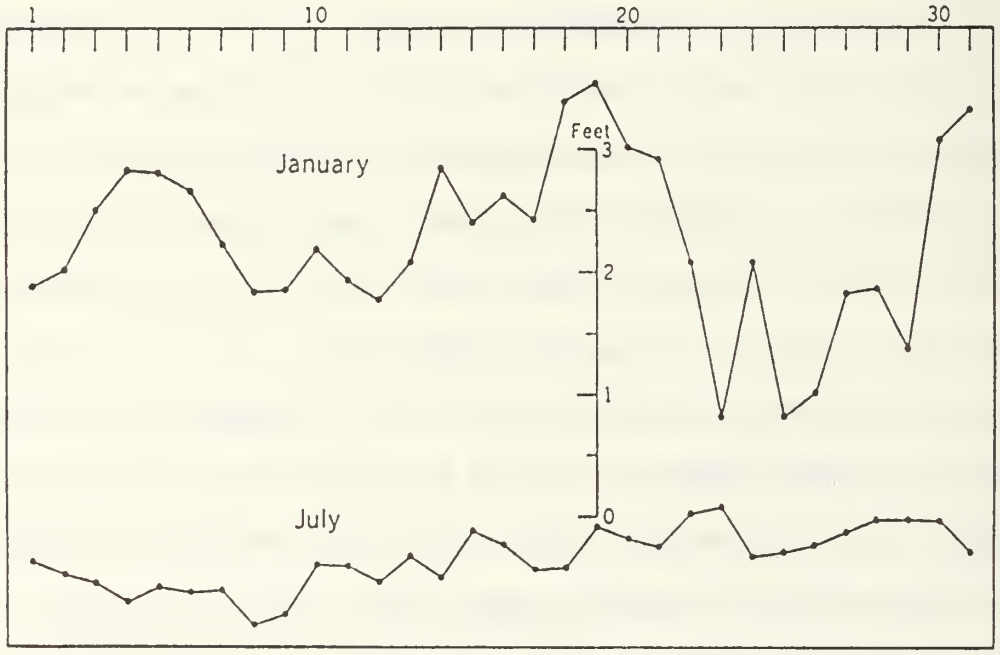

Figure 12. Daily Mean Sea Level Variation. Shows How Daily MSL Variation is Small During Mild Weather. (Marmer, 1951)

weather, the change in SST over a survey period will be on the order of centimeters on the days of greatest SST variation.

3. The Geoid

The ocean geoid is insignificantly variable over survey time scales but may vary by as much as a meter in 30 horizontal kilometers. Over the space scale of the survey the geoid may change by some meters.

4. The Error of a Single Measurement

The total error of a single measurement contains two components of error, as shown at the close of Chapter I. The first error is in the vertical positioning of the airborne platform by GPS, for which we will adopt an accuracy of 5 cm. The second source of measurement error is in the laser derived estimate of MWS. The error from this estimate is thought to be 5 to 10 cm. Since it is assumed that the two error sources are uncorrelated, the worst case total error of a single measurement is;

$$\sigma_T = (\sigma_l^2 + \sigma_p^2)^{1/2} = (10^2 + 5^2)^{1/2} \doteq 11 \text{ cm} \qquad (23)$$

where

σ_T = total error in the measurement of MWS above the ellipsoid
σ_l = error in MWS estimation as determined by the laser altimeter
σ_p = error from GPS derived vertical position.

It is further assumed that the errors are normally distributed. Thus σ_T is one standard deviation.

C. THE CROSSOVER MEASUREMENT

To eliminate all space varying components of η, (the geoidal undulation and SST in particular), the crossover equation needed is;

$$\Delta\eta = (H - h)_{(t=pl)} - (H - h)_{(t=xl)} \tag{24}$$

or

$$\Delta\eta = \Delta H + h_{(t=xl)} - h_{(t=pl)} \tag{25}$$

where

t=pl is the time of principal line crossing at the intersection of the principal and cross lines

t=xl is the time of crossline crossing at the intersection of the principal and cross lines

$\Delta H = H_{(t=pl)} - H_{(t=xl)}$.

ΔH is determined directly from differential GPS carrier phase measurements and $h_{t=xl}$ and $h_{t=pl}$ are LIDAR measured heights. Thus $\Delta\eta$ is a measured quantity with one standard deviation $\approx$ 16 cm (see below). Since the geoid and SST are not time varying, (except for a small linear trend in SST as discussed above), they will drop out of the difference. That which remains is the change in η due to the small time varying effect of SST, the error from 2 measurements (i.e., $[2]^{1/2}\ \sigma_T$ $\approx$ 16 cm), and the largest time varying component of η for survey time scales, ΔTS.

$$GEOID_{t=pl} - GEOID_{t=xl} = 0 \quad (26)$$

and

$$\Delta\eta = \Delta TS + \Delta SST + error \quad (27)$$

where

$$\Delta TS = TS_{t=pl} - TS_{t=xl} \quad (28)$$

$$\Delta SST = SST_{t=pl} - SST_{t=xl} \quad (29)$$

Thus ΔTS (the oscillation due to the tide only), is clearly isolated from the other sources of oscillation within the survey area. With the physical meaning of the observations known, a mathematical model for $\Delta\eta$ is needed. Except where the tidal range is very small, in which case tidal sounding reductions are not required, the signal to noise ratio will always be large for ΔTS.

D. THE MATHEMATICAL MODEL

The proposed model is a sine-cosine series. The arguments for the sines and cosines will be the angular speeds of the tidal constituents thought to be present. Karunaratne (1980) used such a model to smooth data gaps in tidal records. He demonstrated that a sine-cosine series is superior to Lagrangian interpolation for fitting tide data to a curve. He also found, through regression analysis, that even in non-open coast tidal zones (i.e., within small basins), where

shallow water tidal constituents are present, it usually is enough to include only the M_1, M_2, M_4, and M_6 constituents for the best curve fit to the data points (see Schureman, 1971 for an explanation of the above lunar constituents).

If the period of the n^{th} tidal constituent is T_n, then the angular speed is;

$$\omega_n = (2 \times \pi) / T_n$$

The sine-cosine series for η due to tides at some time t is;

$$\eta = A_0 + \sum_{n=1}^{N} A_n(\cos \omega_n t) + B_n(\sin \omega_n t) \tag{30}$$

where

A_0 = the mean sea level determined for the survey period
A_n = the cosine amplitude coefficient of the nth constituent
B_n = the sine amplitude coefficient of the nth constituent
t = time.

Then the change in η due to tides as measured at the crossover point at the time of the principal line crossing and again at the time of the crossline crossover is;

$$\Delta\eta = \sum_{n=1}^{N} A_n\{\cos(\omega_n t_{pl}) - \cos(\omega_n t_{xl})\} + B_n\{\sin(\omega_n t_{pl}) - \sin(\omega_n t_{xl})\} + S\Delta t + error \tag{31}$$

In this model all non-periodic phenomena (including mean sea level), cancel in the crossover difference equation. The amplitude coefficients are unique to the tidal zone in question. The last term, $S\Delta t$ is included to model any linear

trend in SST rise or fall over the survey period. The model would give a perfect fit to the observations if all the constituents present were known, if there were no error in the measurements, and with enough observations (i.e., at least as many observations as unknowns). Since the first condition above is never exactly met in the ALS survey scenario, an approach to minimizing the number of terms to sum over in the model is developed in the next section.

1. Choosing the Parameters for the Model

The next step in the refinement of the model is to choose which tidal constituents to include in the summation. As shown by Karunaratne, rarely do more than four terms improve the result. Since the optimum fit to the model will occur for the fewest number of necessary unknowns, an analysis of those most likely to describe the physical situation follows.

Many of the most important equilibrium tidal constituents fall into two fundamental categories. They are either diurnal with a period of approximately 24 hours or semidiurnal with a period of approximately 12 hours. There are also long period and terdiurnal constituents among others, and knowledge of these is critical for long range tidal prediction. But to fit a set of short period observations to a curve, a model containing only the most basic constituents will give good results. A synodic period is necessary to

separate any two tidal constituents, (Schureman, 1971). The synodic period is given by;

$$(2\frac{\pi}{\omega_1 - \omega_2}) \tag{32}$$

Examination of the expression for the synodic period shows that the nearer any two constituents are in period, the longer the time to separate them in a harmonic analysis. Since a harmonic analysis is a least squares fit to the amplitude coefficients, and this is the method proposed in the next section to find the amplitude coefficients, no two constituents from either the diurnal or semidiurnal categories can be separated in the short time of survey observations. For this reason only a diurnal and semidiurnal constituent need be included in the model. The two most frequently occurring constituents which give the largest variation to the tidal fluctuation are the K_1 and M_2. For the purpose of smoothing $\Delta\eta$ measurements, the difference between the periods of the M_1 and K_1 are not critical and so either may be used to model the diurnal component of oscillation.

In addition to the equilibrium tidal constituents, shallow water constituents are responsible for the unique character of tides in smaller basins. Rarely are these constituents important for the continental shelf tide. Any apriori knowledge from historical tidal records of the constituents present may be used to choose either the equilibrium or shallow water constituents. For instance, if

it is known that the local tide lacks a semidiurnal character, perhaps the M_2 term should be neglected. With apriori knowledge of the presence of shallow water tides, or if there is suspicion they are present, a regression analysis may be employed to see if the inclusion of these constituents in the model improve the fit.

Now that the number of constituents to include in the model has been reduced to a minimum, the number of unknowns has been reduced also. For each constituent there are two unknown amplitude coefficients, A_n and B_n.

E. METHOD OF LEAST SQUARES

To solve for the unknown amplitude coefficients, the criteria of minimizing the sum of the squares of the residuals is used. Equation 31 is the observation equation. The amplitude coefficients are the parameters sought in the least squares solution, and the measured differences of η, (derived from the difference between the two H-h measurements made at the crossover point), provide the observations. In matrix form (Uotila, 1986) gives these equations as, (where all matrices are in boldface type);

$$\mathbf{A}\hat{\mathbf{x}} = \mathbf{l} + \mathbf{V} \tag{33}$$

where

$\mathbf{A}$ is the design matrix
$\hat{\mathbf{x}}$ are the estimated parameters
$\mathbf{l}$ is the observation vector
$\mathbf{V}$ is the residual vector.

Each observation will be given unit weight with the assumption that there is no correlation between observations. Each element of the diagonal weight matrix is then $1/\sigma_T^2$, where σ_T^2 is the total variance of a single measurement. This implies the apriori variance is of unit weight.

The weight matrix is;

$$\mathbf{P} = \sigma_0^2 \, \mathbf{\Sigma}_m^{-1} \tag{34}$$

where

$\mathbf{\Sigma}_m$ = the variance measurement matrix
$\sigma_0^2 = 1.$

With the above defined matrices, the solution is given by

$$\hat{\mathbf{x}} = [\mathbf{A}^T \mathbf{P} \mathbf{A}]^{-1} \mathbf{A}^T \mathbf{P} \mathbf{l} \tag{35}$$

where the $\hat{\mathbf{x}}$ vector contains the estimated amplitude coefficients. The error associated with the estimated parameters, $(\hat{\mathbf{x}})$, are the residuals, defined above.

The variance-covariance matrix of the parameters resulting from the least squares solution is;

$$\hat{\mathbf{\Sigma}}_x = [\mathbf{A}^T \mathbf{P} \mathbf{A}]^{-1}. \tag{36}$$

The aposteriori variance of unit weight is computed as;

$$\hat{\sigma}_0^2 = (\mathbf{V}^T \mathbf{P} \mathbf{V})/\mathrm{DOF} \tag{37}$$

where

DOF, (DEGREES OF FREEDOM) = n-u
n = number of observations
u = number of unknowns or parameters.

The validity of the adjustment can be judged by the aposteriori variance of unit weight as described next. If the mathematical model represents the physical situation well, (i.e., the rise and fall of the tidal zone surface) which gave the observations, if the apriori variance of unit weight was accurate, (i.e., if the total error of a single measurement was accurately estimated), and if there were no obvious blunders in the measurements, the aposteriori variance of unit weight will be close to unity. The confidence interval test for this is;

$$P\left[\frac{\chi^2_{a,dof}\sigma_0^2}{dof} \geq \hat{\sigma}_0^2 \geq \frac{\chi^2_{b,dof}\sigma_0^2}{dof}\right] = b - a \qquad (38)$$

where

a = $\alpha/2$
b = $1-\alpha/2$
b-a = $1-\alpha$
α = the confidence level of the test.

With an understanding of what the observations represent physically, and with a mathematical model now able to be tested for accuracy, we now apply the theory developed to a simulated situation. This is the subject of the next chapter.

V. THE SIMULATION MODEL

A. INTRODUCTION

As stated in the introduction, since no ALS data were available to test the theory thus far presented, a computer simulation of an airborne survey and the results obtained are offered to support this thesis. The computer simulation model was written in FORTRAN 77. The description of the simulation model follows the information flow depicted in Figure 13. The objective of the simulation is to create observations of the type seen in a real ALS survey situation. This was done by taking a known tidal signal and adding a normally distributed realistic measurement error as described in Chapter IV. The tide signal itself was created from a known harmonic cosine series with 14 constituents which was derived from a 366 day harmonic analysis performed on observations from an open coastal tide station. The known tide signal, with the measurement error added, was then analyzed using the limited mathematical model developed in Chapter IV. The signal was sampled as it would be during a typical ALS survey and the resulting "observations" used in a least squares adjustment. The resulting tidal curve is then related to the depths measured in the survey area by means of a datum transfer.

The physical location of the simulated survey area was the 200 km stretch of coastline south of Monterey CA which has

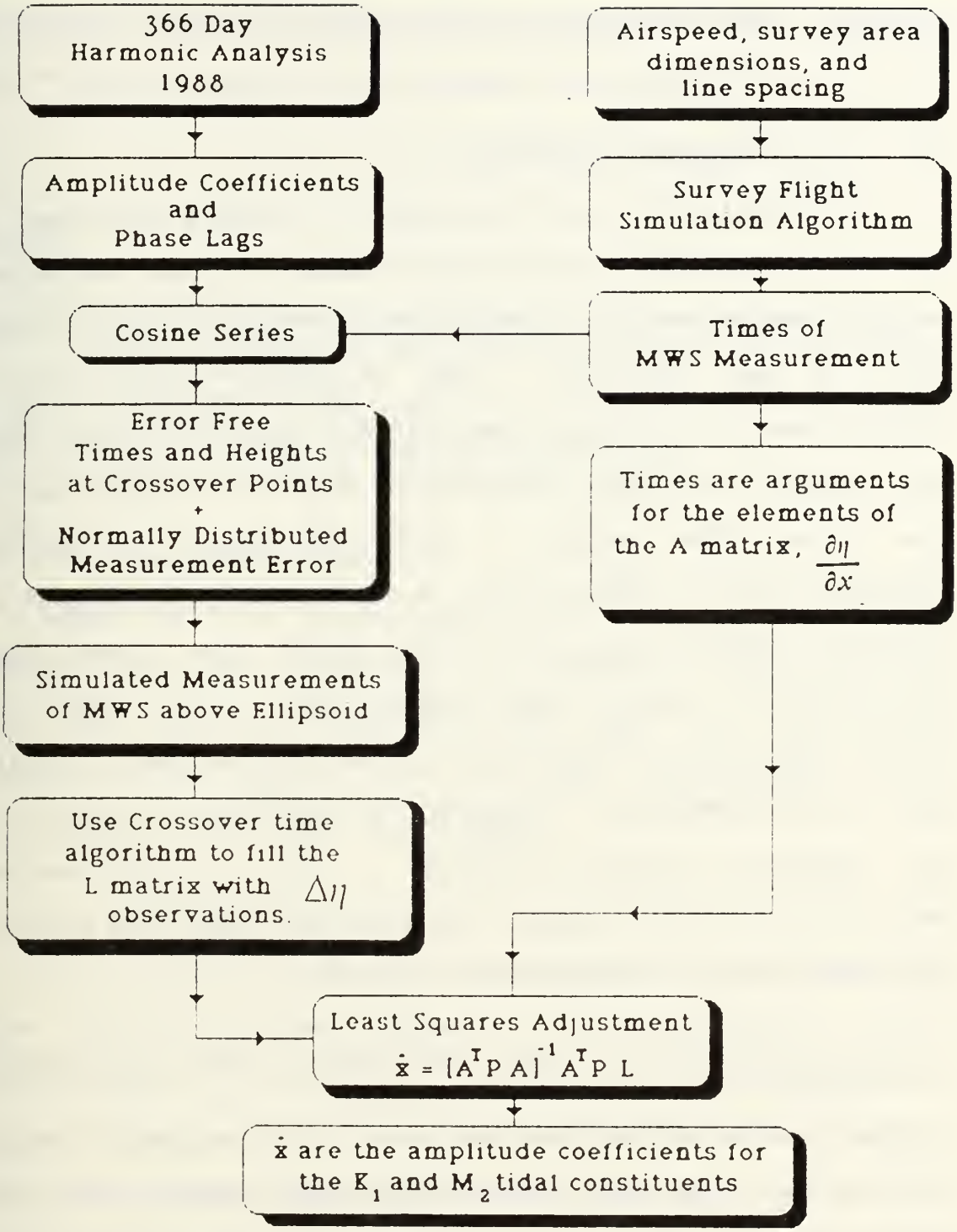

Figure 13. Simulation Model Flow Chart.

Port San Luis CA at the southern edge. The typical survey scenario would suggest that one reference tide gauge be installed at Monterey and operate for at least 30 days.

B. 366 DAY HARMONIC ANALYSIS

The results of a 366 day harmonic analysis performed in 1988 by the National Oceanic and Atmospheric Administration (NOAA), for the coastal tide stations of Monterey and Port San Luis, CA were obtained. NOAA routinely solves for 37 constituents in a harmonic analysis and reports the amplitude coefficients, and phase lags to be used in a cosine series that gives tide heights. Each constituent is further evaluated for its reduction of variance (i.e., the amount of variation from the mean value which the constituent contributes). Only those constituents which contribute greater than 1.5% variance are included in the cosine series used in the simulation. Appendix A contains the results of the harmonic analysis obtained. For a comprehensive description of the harmonic analysis performed and results provided by NOAA, see Schureman (1971).

C. THE COSINE SERIES WITH MEASUREMENT ERROR, A FORTRAN FUNCTION

The cosine series was used in a non-intrinsic FORTRAN function which gave the tide heights with measurement error above a reference plane. The source of the time argument was

the flight simulation program described next. The following symbology is used in the cosine series which has 1 JAN 1988 as t=0;

$$\eta = A_0 + \sum_{n=1}^{N} R_n(\cos \omega_n t - \zeta_n) \tag{39}$$

where

η = the instantaneous sea level above the reference plane, (either reference ellipsoid or zero of tide staff)
n = nth constituent
A_0 = the height of mean sea level above the reference plane
R_n = amplitude coefficient
ω_n = angular speed of the nth constituent
ζ_n = phase lag of nth constituent.

D. THE MEASUREMENT ERROR

Added to this cosine series was normally distributed pseudorandom error produced by a computer library routine. The mean value of this noise was zero and the standard deviation was equal to the total measurement error, (σ_T = 11 cm), from the last chapter.

E. THE REFERENCE PLANE

The reference plane is the plane the MWS is referenced to. The reference plane chosen is inconsequential to the observations as long as it is accurately recoverable. The A_0 term of Equation 30 represents the constant vertical distance from the reference plane to the mean sea level value and is differenced away in the crossover equation,(i.e., $\Delta\eta$, Equation 31). Thus a reference surface is used only as a

means of identifying the change in MWS over time and so must be recoverable with known accuracy from one measurement to another. In the simulation the zero of the Port San Luis tide staff was used as the reference plane so that the chart datum resulting from the datum transfer could be compared with the true chart datum which is known at this staff. It will be seen during the datum transfer discussion that the MWS measurements are considered as the individual tide heights for sounding reduction. With the amplitude of the tide signal known in relation to the chart datum at the time of depth measurement, the measured depth need only be "reduced" by the vertical distance from the chart datum to the MWS.

F. THE SURVEY FLIGHT SIMULATION PROGRAM

It is appropriate at this juncture to note an element conspicuously absent in the flight simulation program. Apart from the fact that it cannot anticipate every operational problem associated with the collection of the necessary data, the model does not simulate the spatial movement of the aircraft over the survey area. The simulation includes only temporal progress. The implications of this absence are discussed at length in the next chapter and shown to be advantageous rather than being a shortcoming.

In order to match the flight progress in time with survey measurements made at the crossover point, (the intersection of the principal and crosslines), the cosine series providing

the tide signal was supplied a time argument which corresponded to the aircraft motion through the survey area. The times were supplied by a flight simulation algorithm. The information needed to produce the simulated times were the measurement platform speed, (P-3 aircraft speed), the alongshore and offshore survey area dimensions, and the principal and cross line spacing.

The aircraft speed used in the simulation was 100 m per second, the low end of the P3 Orion speed range of 100 to 130 m/s. The survey area dimensions were 200 km alongshore by 1 km offshore and the principal line spacing was 250 m and the crossline spacing was 2500 m. The first set of times produced correspond to the aircraft position at the crossover points along the principal lines. The second set of times correspond to the times of the aircraft location at the crossover points along the crosslines. Refer to Figure 14 during the following discussion.

1. The Crossover Measurements along the Principle Lines

The following formula was used to simulate the aircraft travel along the principal lines;

$$t_{pl} = xls/as$$

where

t_{pl} = the time of aircraft horizontal co-location with the crossover point along the principal lines.
xls = crossline spacing
as = airspeed.

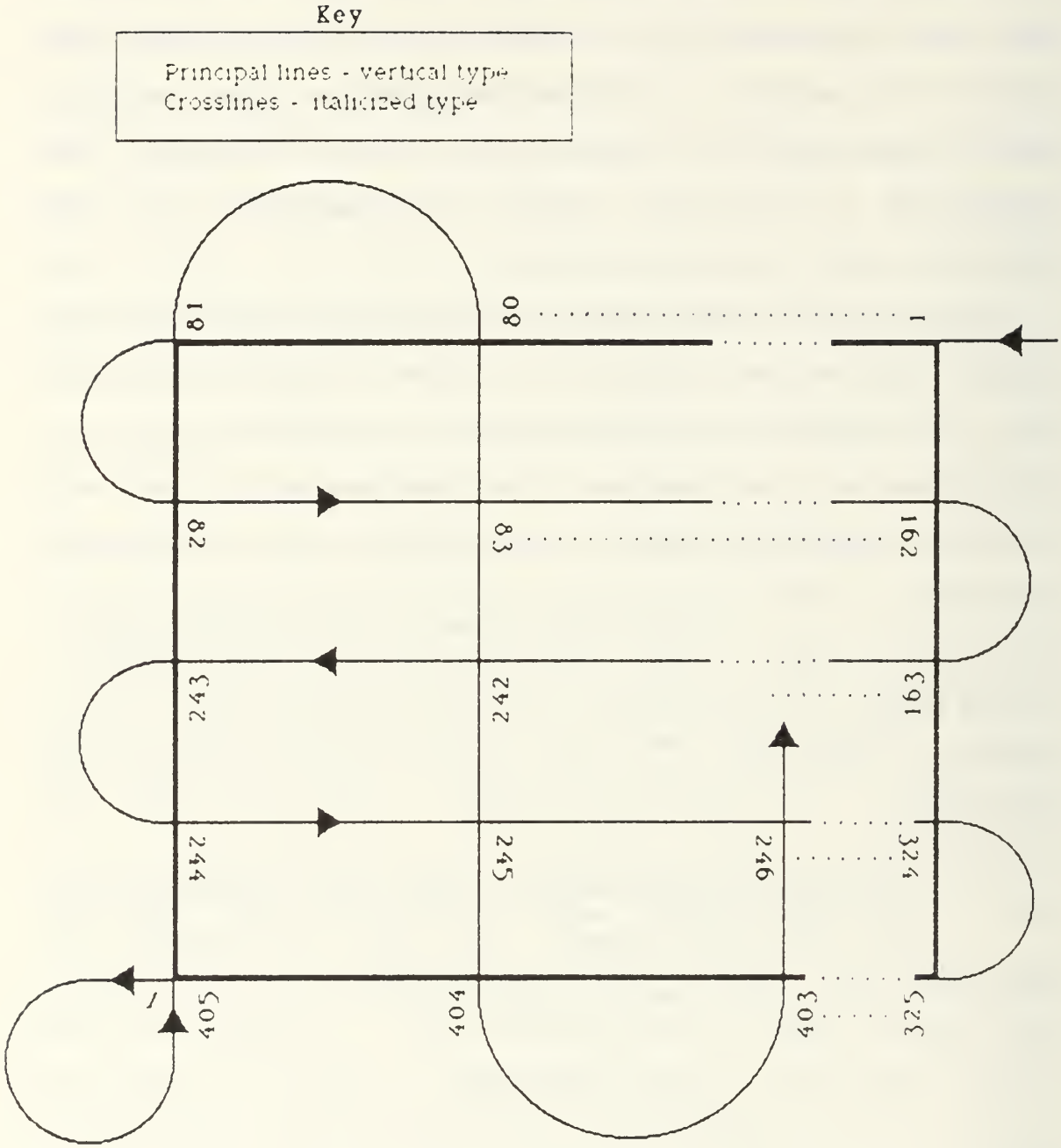

Figure 14. Incrementing Array Elements

This relation gives the time required by the aircraft to travel between crosslines along the principal lines. The initial time of the survey (i.e., t_0) was arbitrarily chosen as 0000 hours 1 April 1988. Since the survey area was 1 km wide in the offshore direction, and since the first principal line is run along the inshore survey area border in the alongshore direction and the last principal line along the offshore survey area border also in the alongshore direction, with 250 m principal line spacing there will be five principal lines. The first crossline runs along the survey area border in the direction perpendicular to shore, and each subsequent line is run 2500 m into the survey area, yielding 81 crosslines. This gives 405 crossovers, 81 for each of the five principal lines. Starting at t_0, each succeeding crossover point occurred 25 seconds later along the principal lines. At the end of each line, five minutes was allowed for a turn. These times were stored in an array. Next these times were reordered and written to file with a tide height measurements corresponding to each time. As the algorithm identified a crossover point which occurred along a principal line and on a particular crossline, the time was used as an argument in the cosine series function described above. Thus the times and simulated measured heights corresponding to the five principal line crossings of crossline 1 were ordered in the file sequentially, as were the five principal line crossing times and heights for each subsequent crossline.

2. The Crossover Measurements Along the Crosslines

Since the survey area is only 1 km wide, each crossline requires only 10 seconds. Because the cosine series simulated η measurement of Equation 39 will not change over 10 seconds, only one η value was recorded for each crossline. For evaluation of survey areas with a wider offshore dimension, the time corresponding to each crossline is the time the aircraft would have been midway through the crossline. Thus if the survey area had been 10 km wide, the algorithm would have recorded the time midway through the crossline, (i.e., 1/2 x crossline length ÷ airspeed = 500 seconds), to add accuracy to the model. Since the tide does not change appreciably in 1000 seconds, the mid-crossline time gives a slightly more representative η measurement for the whole crossline. Five minutes plus the time to traverse between adjacent crosslines was allowed for turns, (i.e., 5 minutes 25 seconds).

As these crossline times were generated they were used as an argument in the cosine series function and the times and heights were written to the crossline time and height file.

G. FILLING THE LEAST SQUARES ADJUSTMENT MATRICES

The matrices described in Chapter IV paragraph E were then filled. The $\hat{\mathbf{x}}$ vector is the estimated amplitude coefficients of $\Delta\eta$ (i.e., A_n's and B_n's of Equation 31).

$$\hat{x} = \begin{bmatrix} A_1 \\ B_1 \\ A_2 \\ B_2 \\ \cdot \\ \cdot \\ \cdot \\ A_N \\ B_N \end{bmatrix} \tag{40}$$

The A matrix or design matrix has as many columns as there are parameters and as many rows as there are observations. With temporal arguments corresponding to the crossover times (i.e., t_s and t_{pl}), it becomes a matrix of scalars.

n = number of parameters = number of columns
m = number of observations or crossover points

$$A = \begin{bmatrix} \cos(\omega_1 t_{pl}) - \cos(\omega_1 t_{xl}) & \sin(\omega_1 t_{pl}) - \sin(\omega_1 t_{xl}) \ldots \cos(\omega_n t_{pl}) - \cos(\omega_n t_{xl}) & \sin(\omega_n t_{pl}) - \sin(\omega_n t_{xl}) \\ & \cdot \\ & \cdot \\ & \cdot \\ & m \end{bmatrix} \tag{41}$$

These times are read from the two time and height files described above, the principal line times, (t_{pl}) and the crossline times, (t_{xl}).

Within the same loop both the heights (η's) are read. These measurements are differenced to give the observations, (i.e., Equation 24), filling the l or observation matrix.

$$l = \begin{bmatrix} obs_1 \\ obs_2 \\ obs_3 \\ \cdot \\ \cdot \\ \cdot \\ obs_m \end{bmatrix} \qquad (42)$$

where obs = $\Delta\eta$, Equation 24.

With the matrices filled, the subroutines that perform the transpose, inverse, and matrix multiplication functions are called to compute the least squares adjustment which yields the estimated parameters, $\hat{\mathbf{x}}$.

H. THE DATUM TRANSFER

Having estimated the amplitude coefficients of the major tidal components in the survey area, it now remains to link these to some defined tidal datum. This may be done by a datum transfer technique. The datum transfer method used in the simulation model is after the datum transfer technique for "sketch surveys" from the Admiralty Tidal Handbook No. 2, N.P.122(2), 1975. The method is recommended for datum transfer from a reference or "standard port" tide staff to a tide staff used for a very short period survey (i.e., less than a day and if possible with at least one high and one low water recorded).

The transfer is accomplished as follows;

- compute the range of the tide at the reference station during the period of the survey
- compute the range of the tide in the survey area, (this is done by generating a curve using the amplitude coefficients obtained in the least squares adjustment in the equation for η, Equation 30)
- obtain the range ratio, the ratio of the range in the survey area to the ratio of the range at the reference station
- compute the equivalent range (ER), this is done by computing mean sea level for the survey period at the reference gauge and finding the vertical distance on the reference staff to the chart datum. This distance is multiplied by two and multiplied by the range ratio. Half ER is the estimate for where the chart datum lies below the mean value computed on the survey area staff.

The parameters resulting from the least squares adjustment can be used in Equation 30, to give a curve for the survey period. The A_0 term, mean sea level, is not known in relation to the datum reference surface. By using the range ratio method, the datum transfer is not biased by the shortness of the span (e.g., 12 hour) of the LIDAR survey. Errors do occur, however, when the short period range ratio is not representative of the long period range ratio. In other words errors may occur if the range at the reference station does not always change in proportion to the range in the survey area. This is less likely to occur along a smooth continental shelf as defined in Chapter III. These errors are discussed in Chapter VI.

I. SOUNDING REDUCERS

The final product of the simulation model is the depth sounding reducer. The time of depth measurement is used in Equation 30 to give the tide "reducer." The result is subtracted from the measured depth to reduce the depth to chart datum. Since the chart datum is normally a low water datum, most of the tide heights will be above the chart datum. The equation for this is;

REDUCED DEPTH = MEASURED DEPTH - TIDE HEIGHT ABOVE CHART DATUM.

The largest source of error in this equation will be shown in the next chapter to be due to the LIDAR determined MWS measurement. Recall that the time required for the LIDAR signal to return from the MWS is subtracted from the time required for the LIDAR signal to return from the ocean floor and this time is halved and multiplied by the estimated speed of light through the local water column to give the instantaneous depth. This depth must be adjusted for the instantaneous tide height relative to the chart datum. It is the MWS which must be shifted the requisite vertical distance toward the chart datum to give the "reduced" depth.

If there is no error due to the datum transfer and if the model gave a curve identical to the true curve, the error in the sounding reduction would be the error of the LIDAR range measurement alone. The LIDAR range measurement was estimated

to be 5 to 10 cm in Chapter IV. Since this error is known, the examination of the errors which are due to the datum transfer and the error due to the discrepancy between the model curve and the true curve remains. These errors are discussed quantitatively in the next chapter.

VI. RESULTS

A. INTRODUCTION

The results of the adjustment performed on the simulated survey observations are presented in this chapter and the magnitude of the error is analyzed. At the close of the last chapter it was shown that the three sources of error in the final sounding reducer are;

- the error of the model in reproducing the oscillation of the actual multi-constituent tide curve
- the error due to datum transfer
- the normally distributed error arising from the LIDAR determined MWS.

The first result examined reveals how well the mathematical model can represent the oscillation of the actual multiple constituent tidal signal. Secondly, we examine the error resulting from the datum transfer and show how the errors of model fit and datum transfer combine. Finally the total error from the datum transfer, mathematical model, and LIDAR determined MWS measurement are evaluated to show that the tide reducer applied to the LIDAR depth sounding meets IHO specifications for agreement within 0.3 m with the actual tide.

B. THE MODEL ERROR

In this section the oscillation of the model is compared to the true tide curve oscillation by plotting the two together. By giving the model derived curve the same mean value (i.e., A_0 from Equation 30), as the true harmonic series curve, the amplitude and frequency of oscillation around a common mean level can be compared. Such a comparison reveals how well the mathematical model approximates the true harmonic series curve derived from a 366 day harmonic analysis.

Recall that the aposteriori variance of unit weight resulting from the adjustment should be very nearly unity if the following conditions were met in the adjustment;

- the total error term σ_T is accurately estimated
- there are no blunders in the observations
- the mathematical model describes the physical phenomena well.

The aposteriori variance of unit weight for this adjustment varies depending on the seed used for the pseudorandom error routine but is always very close to one. The worst aposteriori variance of unit weight result was 0.87 which can be shown to be the same as one by Equation 38 with a confidence of 95% (i.e., $1-\alpha=95\%$). Since we can be certain that the first two conditions listed above are met because the simulation model includes only the total σ_T error and no blunders, it appears that the mathematical model with only two constituents can describe the harmonic series with 14

constituents well judging by the aposteriori variance of unit weight. This is illustrated in Figure 15. This plot shows the harmonic series curve for Port San Luis, CA supplied by NOAA plotted against the adjustment model curve. There is a tendency for the model to situate the curve slightly higher than the true curve. The reason for this is not known for certain. In tests done to investigate the problem it was shown that the adjusted curve "floats" higher above the true curve as the normally distributed σ_T increases. For the σ_T used in the simulation, the "float" error resulting is on the order of 0.1 foot, which is so small it need not be eliminated for satisfactory results.

Referring to Figure 16, it can be seen that the model also fits the harmonic series curve supplied by NOAA for Monterey, CA. The curve plotted for Monterey is shifted in time by 26 minutes so that the curves can be compared for oscillation only. The high degree of agreement between the curves illustrates that the amplitude coefficients derived from observing tides at Port San Luis apply to Monterey but the shift in time shows that there is a phase lag. The fact that the two curves oscillate around the same mean value is coincidence. Mllw at Monterey is 2.923 feet below mean sea level (msl) while mllw is 2.809 feet below msl at Port San Luis. It just so happens that the model "float" error is 0.1 feet and the difference in mllw at the two stations is about 0.1 feet. If it were not for this coincidence the two curves

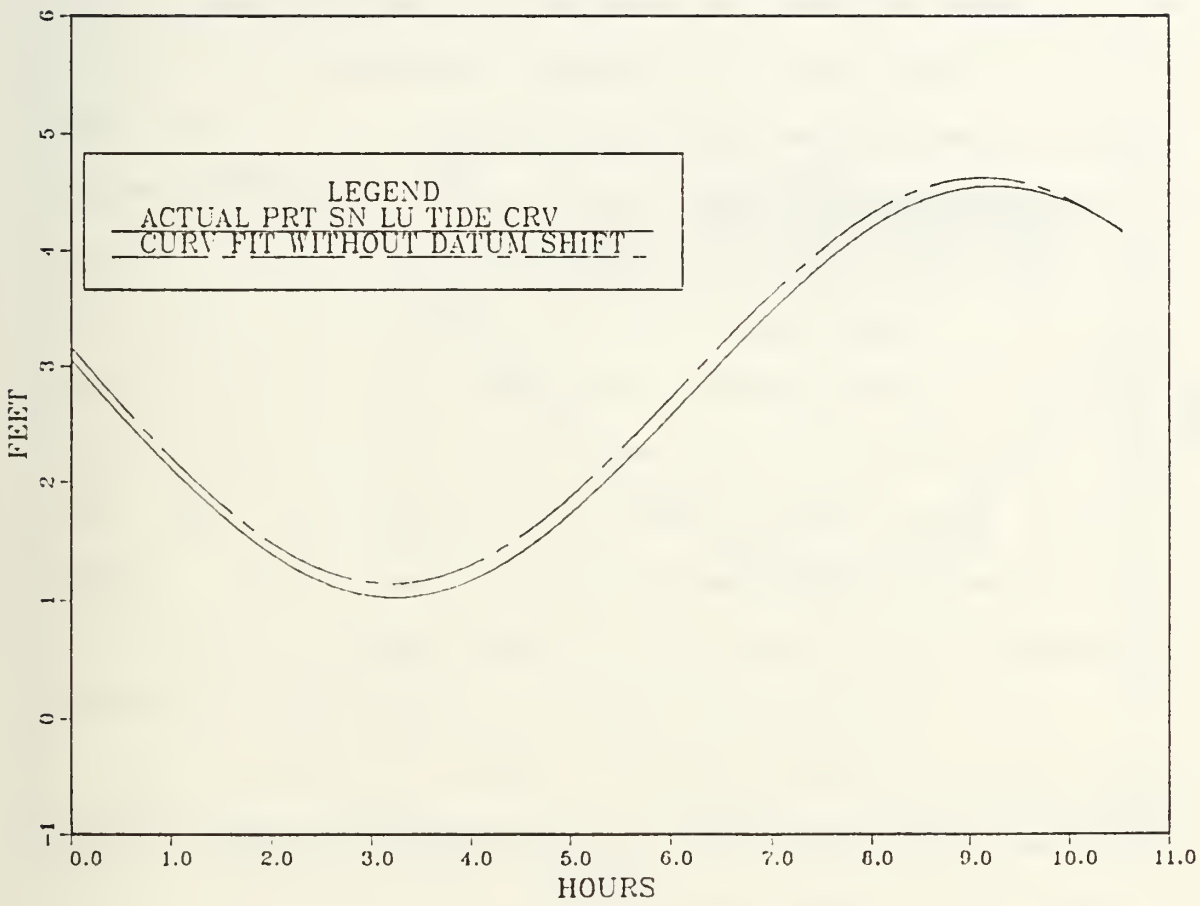

Figure 15. Model Results versus True Port San Luis Tide Curve. (True Curve from NOAA's Harmonic Analysis)

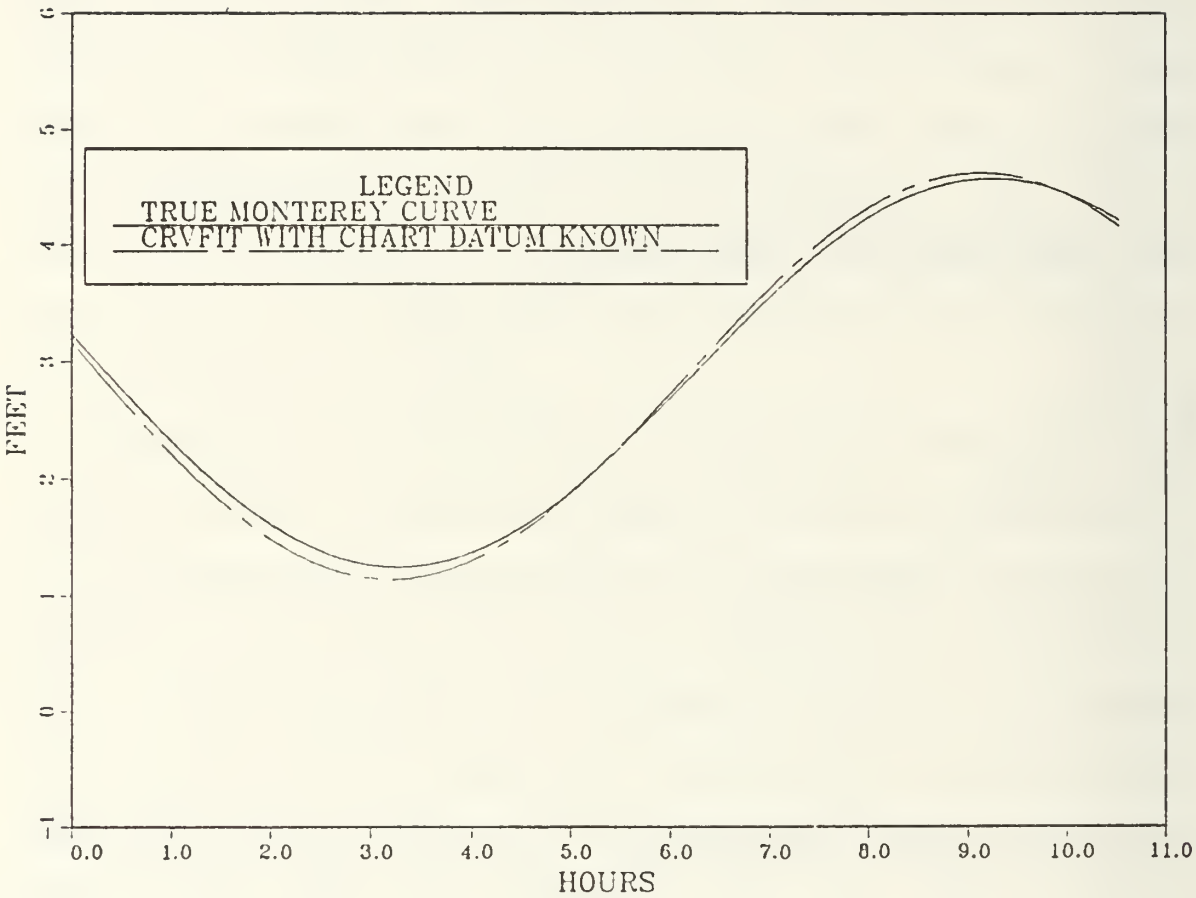

Figure 16. Model Results versus True Monterey Tide Curve (Monterey Curve Shifted 26 Mins in Time).

would have to be demeaned to show they oscillated with the same frequency and amplitude. This coincidence does demonstrate however that the oscillations at the two borders of the survey area are nearly identical in frequency and amplitude, although different in phase. The phase difference can be approximated in the case at hand by examining the approximate alongshore distance of the survey area and comparing it to the wavelength of the shortest wave of tidal frequency present. The shortest wave at the M_2 frequency as stated in Chapter III, Paragraph C, is the Kelvin wave. This wave also contributes most of the amplitude to the semi-diurnal portion of the mixed tide present along the California coast. The length of the survey area is only 2.5% of this wave (i.e., ~200km/8000km) and so 9 degrees of the total 360 degrees. It will be shown that tide height differences from one end of the survey area to the other do not exceed IHO specifications despite this phase difference.

The next test is to see if the mathematical model agrees with the measured heights well. The measured hourly heights were also obtained from NOAA for both Monterey and Port San Luis. Figure 17 shows a plot of the model curve against the measured heights for Port San Luis. There is very good agreement here as well.

The conclusion to be reached is that the model curve derived from this survey time period, (10.6 hours), with only two constituents (i.e., the K_1 and M_2) agrees very well with

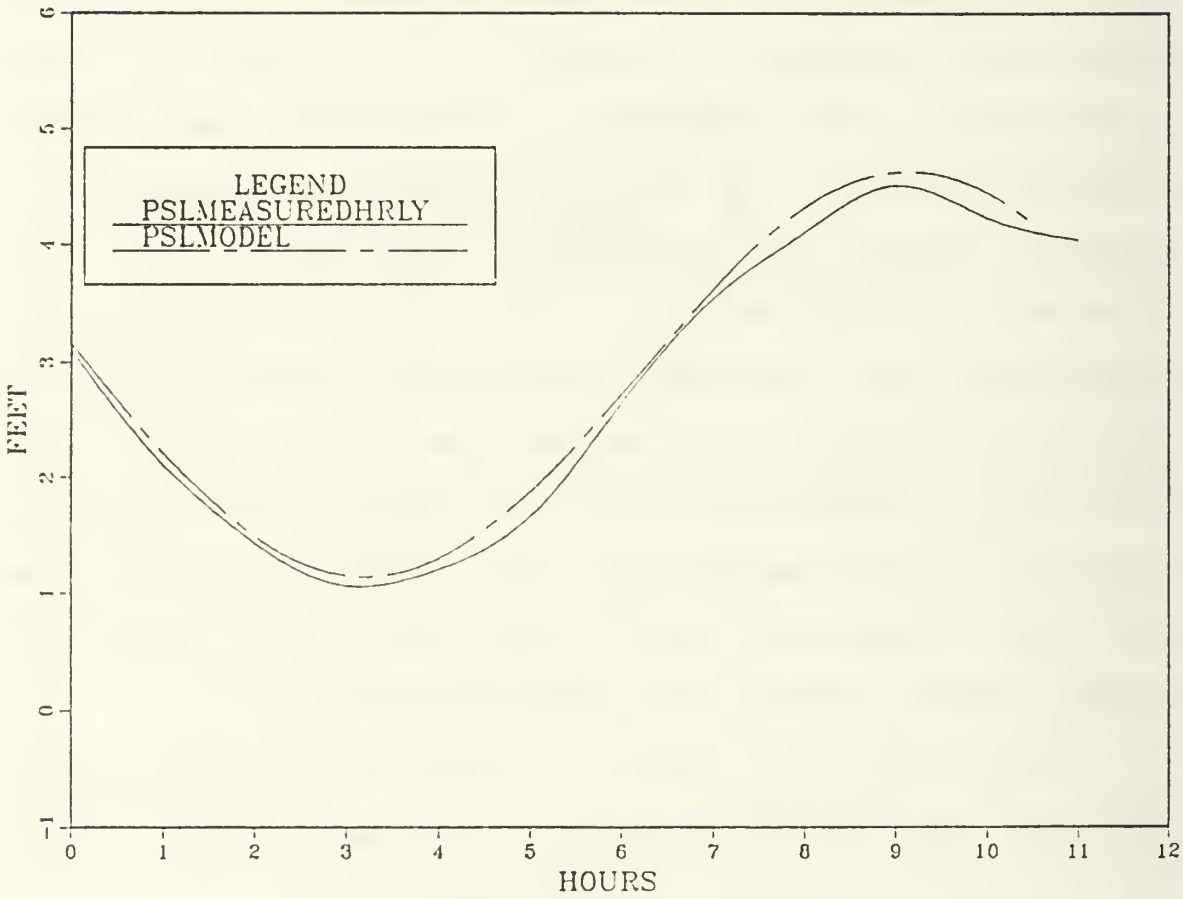

Figure 17. Model Results versus Measured Hourly Heights at Port San Luis.

a real tide curve, whether from a harmonic series or measured hourly heights. Later in this chapter the shortest length of time over which observations can give a good adjustment result will be discussed.

C. THE ERROR FROM DATUM TRANSFER

In an actual ALS survey the curve derived from the model must be related to the chart datum before it can be applied to the measured depths. In this section the error due to the datum transfer will be shown quantitatively. The datum transfer method described in the last chapter was applied as if Monterey was the reference tide station and the area from Monterey to Port San Luis was the survey area. The datum transfer was made to Port San Luis tide staff and the transfer error was -0.15 feet or -0.045 m. The datum transfer method relies on the range ratio derived during the survey period to be representative of the range ratio over a long time period. The range ratio obtained will be representative if the two stations are located along a smooth continental shelf as defined in Chapter III.

With the error of the datum transfer, Figure 18 shows the model tide heights with the chart datum (less than -0.15 foot) transfer applied compared to the true tide curve at Port San Luis. The fit is nearly perfect only because the model "float" error and datum transfer error almost cancel each other. Figure 19 shows the same datum shifted model curve

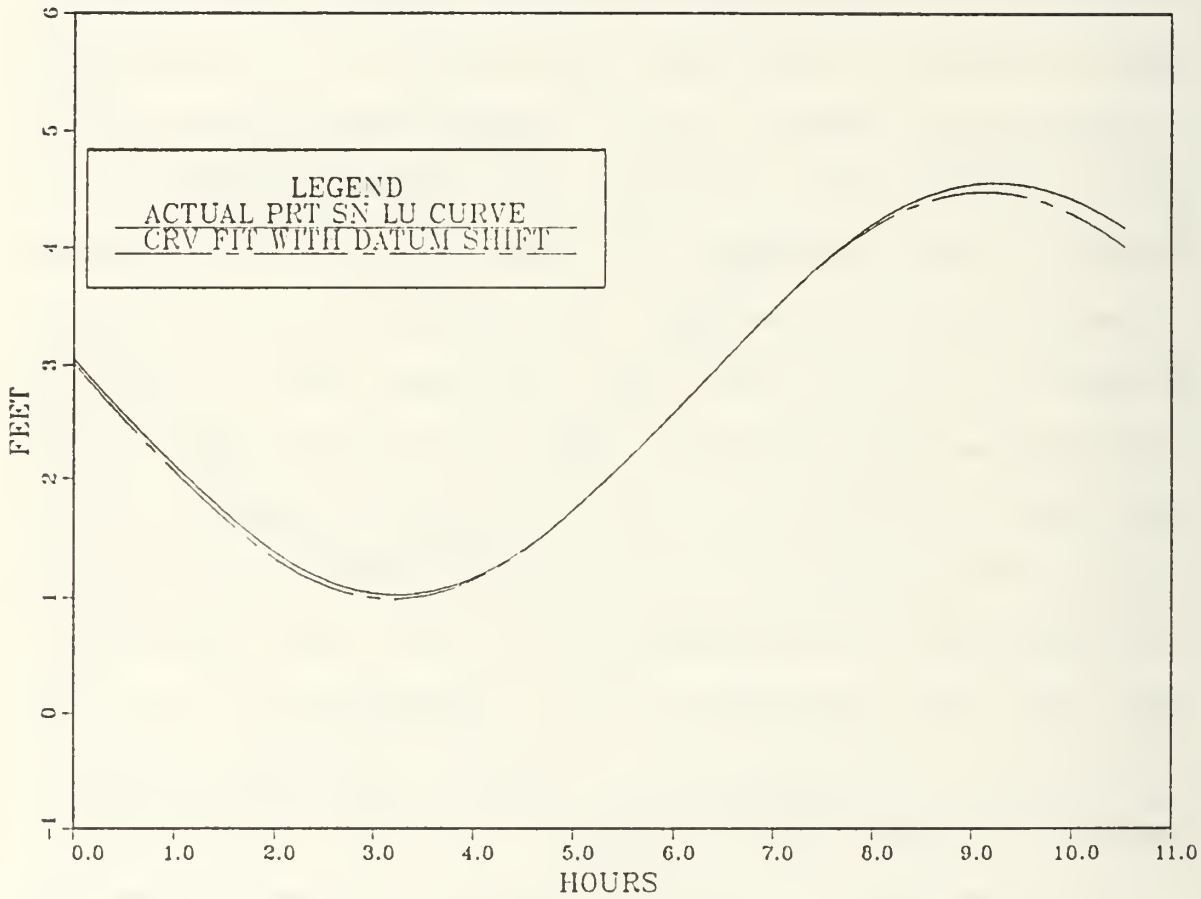

Figure 18. True Port San Luis Tide Curve versus Model Curve with Datum Shift.

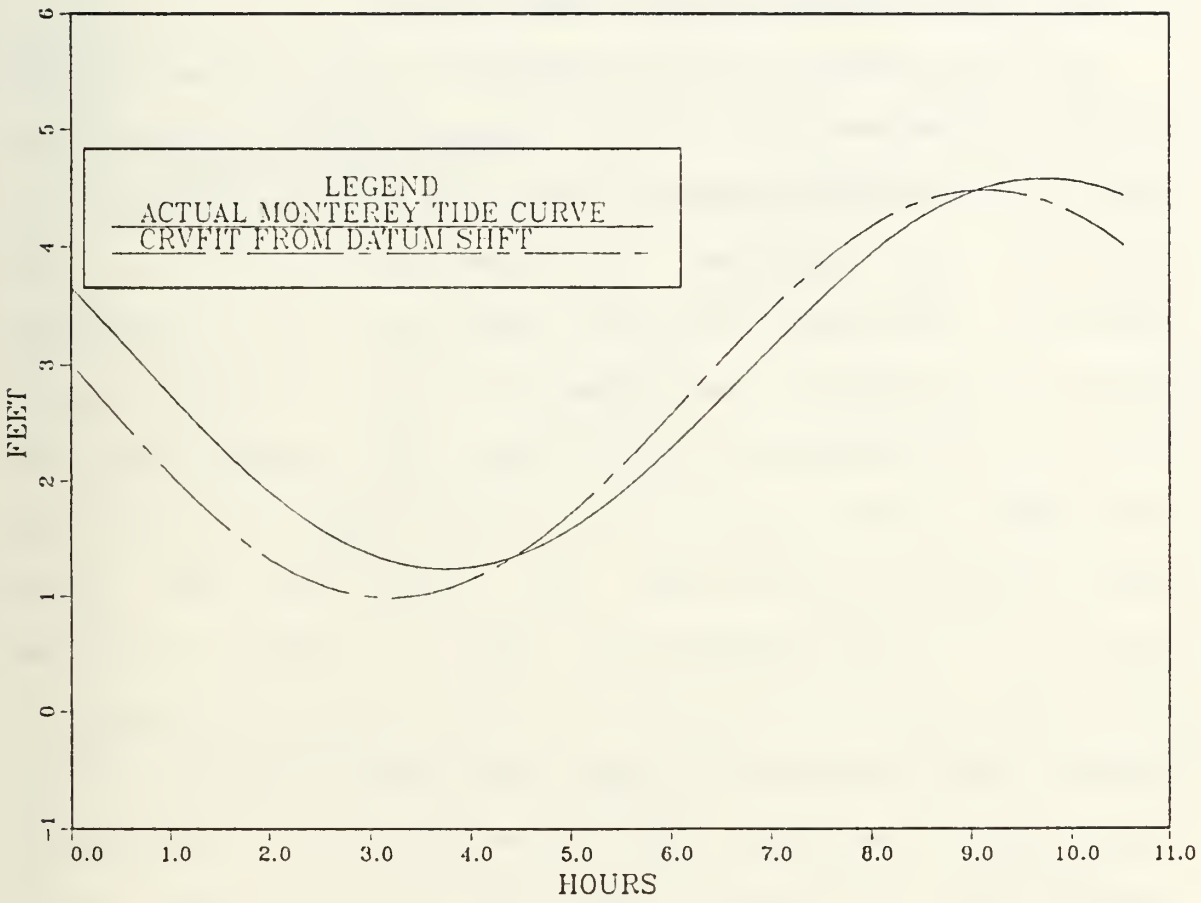

Figure 19. True Monterey Tide Curve versus Model Curve with Datum Shift.

plotted against the true Monterey tide curve. Here the error is primarily due to the phase lag over the distance of separation between the two stations. The magnitude of the differences are under 1.0 foot 100% of the time. This more than meets the requirement specified by the IHO for measuring tides.

D. THE TOTAL ERROR FROM ALL THREE SOURCES

The final question to be resolved is; when the model tide heights are referenced to the transferred chart datum, and are applied to the depths measured, how much error is there in the resulting tidal reducers. The three error sources for the sounding reductions have been quantified for this example along the California coast between Monterey and Port San Luis. The standard deviation of the normally distributed LIDAR MWS measurement error, (σ_T), is 11 cm, and the error from the datum transfer is -0.15 feet. The "float" error, due to the lack of fit of the mathematical model, is worst at Port San Luis, and is about a constant 0.1 foot as shown in Figure 14. When all three sources of error are combined only 1% of the tide reducers resulting from the model are 0.3 m different from the true tide heights above mllw at Port San Luis. Four percent of the model tide reducers are different from mllw on the Monterey tide staff by 0.3 m. These two cases are shown in Figures 20 and 21 respectively.

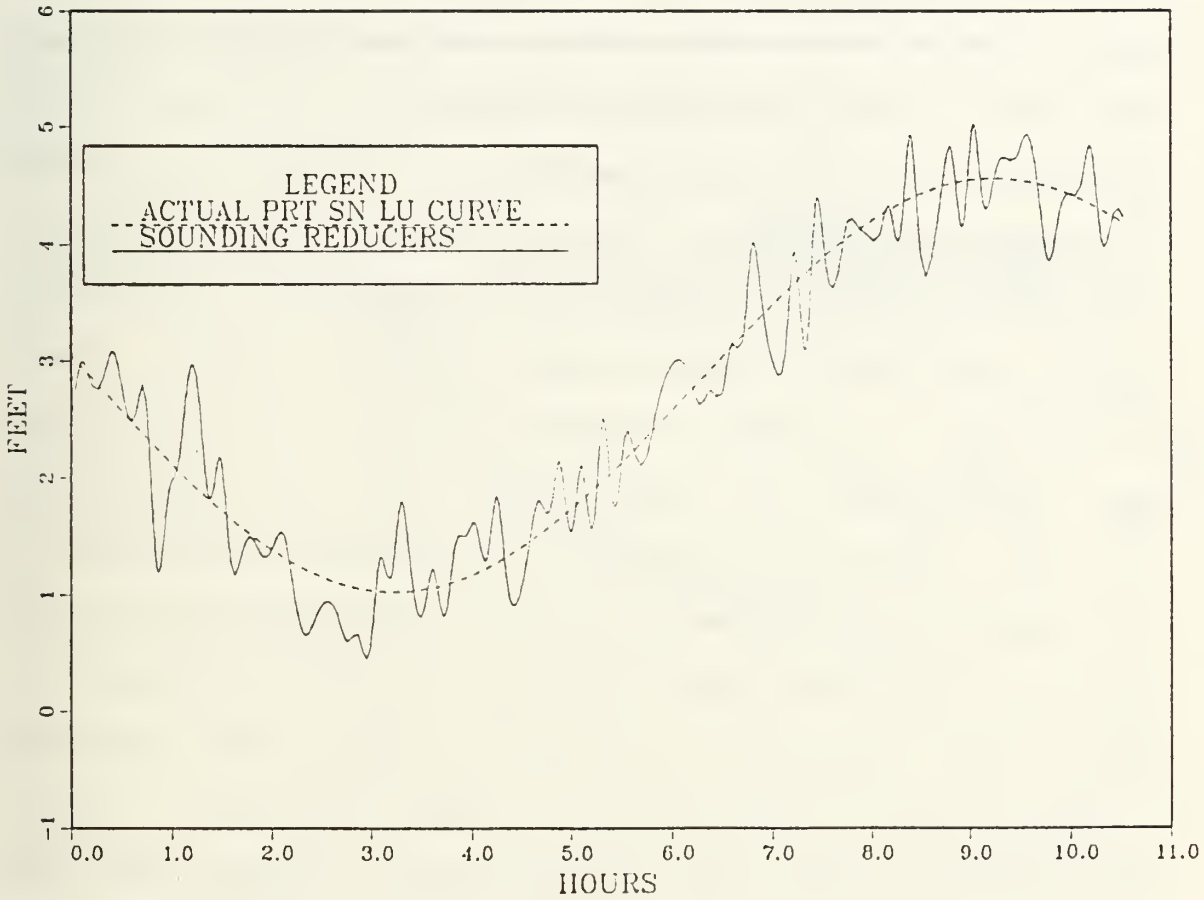

Figure 20. Tide Reducers for Port San Luis (1% of Tide Reducers Greater Than 0.3 m of True Reducers).

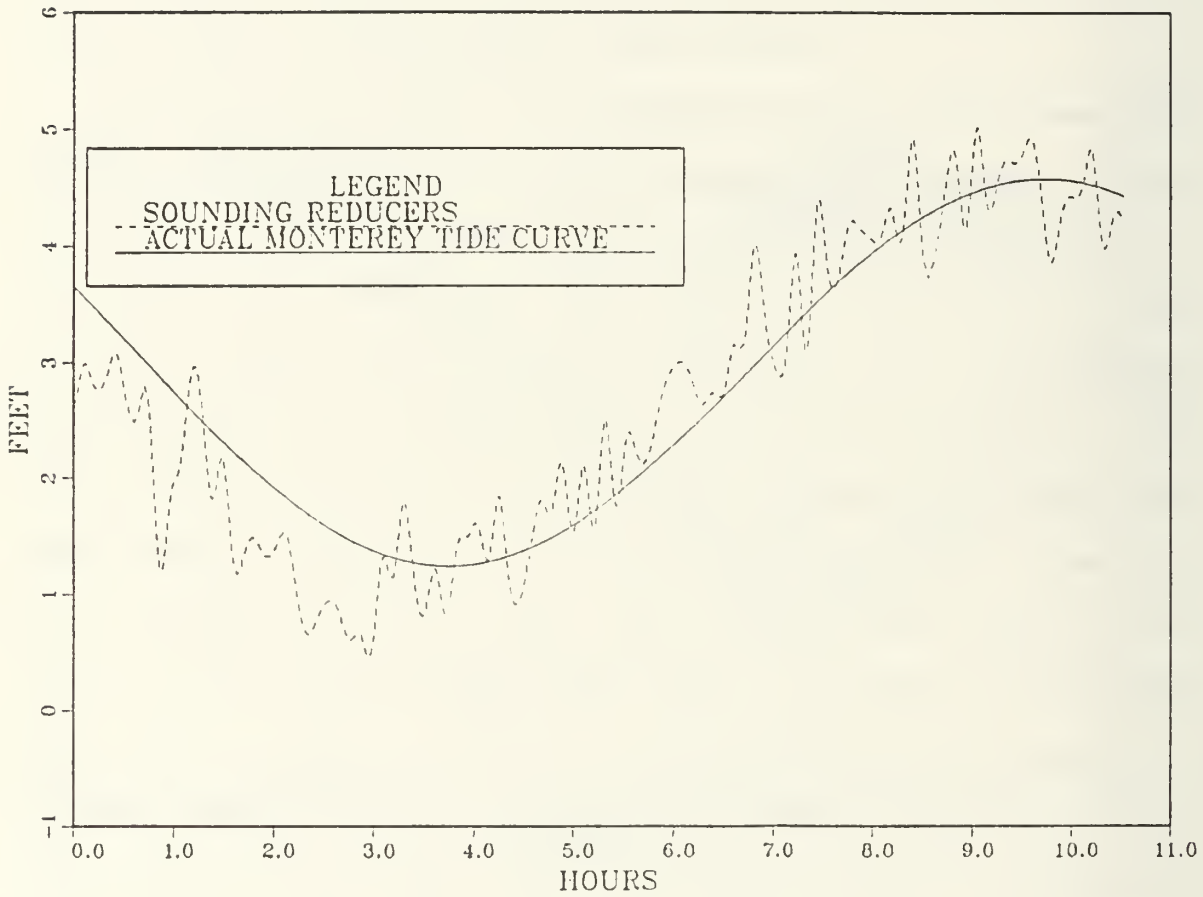

Figure 21. Tide Reducers for Monterey (4% of Tide Reducers Greater Than 0.3 m of True Reducers).

VII. CONCLUDING REMARKS

A. MERITS OF THE SIMULATION MODEL

In the last chapter it was noted that the simulation presented is missing horizontal aircraft movement. Instead, all the observations used in the adjustment are based on the actual oscillations at the pier where the Port San Luis tide station is located. According to the theory presented in Chapter III, these oscillations are characteristic of the entire tidal zone which is at least as large as the survey area. Figure 16 above showed that the amplitude of the oscillations are nearly identical from one border of the survey area to the other. Had the observations been symmetrically distributed throughout the survey area, the amplitude coefficients resulting from the least squares fit would have given a sine-cosine series curve which was more representative of the oscillations of the water level in the center of the survey area. The resulting sounding reducers are most accurate in the center of the survey area but have less error when applied at the borders than the worst errors which resulted in the simulation derived sounding reducers. The results of the simulation model have exceeded the IHO specifications with the worst possible spatial distribution of observations.

B. ADDITIONAL TESTING

The method of determining tidal reducers from airborne bathymetric data proposed in this thesis is not fully proven. Several factors critical to ALS survey applications remain untested. These include the following scenarios which it is proposed be investigated;

- An attempt should be made to transfer the Monterey datum to the next survey area, south of the current test area. This area would extend from Port San Luis to Santa Monica and use the tide staff at Santa Monica as the test for datum transfer error.

- Test the amplification factor in the test survey area. This can be done by multiplying the amplitude coefficients from an existing tide model for the California coast by the amplification factor and comparing the result to the coastal tide gauge measurements.

- The same test made on the coastal California survey area should be performed on an area along the North American east coast. The continental shelf is wider along the east coast providing a considerably different physical setting.

- Within the test survey area the tide is classified by NOAA as mixed. Technically this means the ratio of the $K_1 + O_1$ to $M_2 + S_2$ amplitude coefficients is between 0.25 and 1.50. A mixed tide gives two highs and two lows daily but they are not equal in range. Thus the chart datum is the mean of the lower of the two low tides each day for some time. The method should be tested in areas with other types of tides, (i.e., diurnal and semidiurnal). The chief difference in applying the method to these other tides should prove to be the length of time over which observations are needed. In several tests done on the mixed tide, it appears that the shortest time for which observations yield accurate amplitude coefficients is six hours. This six hour period must include one high and one low water. Further, the observations must be spaced in time to guarantee they have information showing water level change. The possibility exists that the value of $\Delta\eta$ given by Equation 24 is smaller than the total tidal amplitude for all observations. This situation was avoided in the simulated survey by distributing the observations adequately. If the above described sampling problems are avoided, accurate amplitude coefficients may be obtained.

- An attempt should be made to improve the spatial resolution of the tidal zone. This would require the survey area be subdivided into smaller area tidal zones. Each zone must have enough observations and these observations must span the requisite time period and contain information on the full tidal range excursion. On preliminary examination of the observation distribution in the survey simulation, this seems possible.

- The minimum value of the signal to noise ratio (i.e., the ratio of the tidal range to the total measurement error, σ_T), which yields accurate amplitude coefficients should be measured. This would provide information for deciding where to use airborne bathymetric data to obtain tidal heights and where tide gauges are needed.

- Research of the literature to find the areas of the world where the method proposed in this thesis may be applied. Many of the continental shelves where the theory of Chapter III apply have been identified in Clarke and Battisti, 1981.

- Finally, but perhaps most importantly, the method must be used in an actual test survey to discover any operational problems overlooked in the simulation.

C. ALS DERIVED TIDAL REDUCERS VERSUS CONVENTIONAL TIDE GAUGE DERIVED TIDE REDUCERS

In Admiralty Tidal Handbook No. 2, N.P.122(2), 1975, it is recommended that a tide gauge be installed no less than every ten miles along an open coast for hydrographic survey control. Along smooth continental shelves as defined by Clarke and Battisti, coastal tide measurements made with this spatial separation may actually be misleading as to the tidal reducers to be applied away from the shore. Tide gauges are typically located in protected areas for ease of installation and maintenance. Referring to Figure 9, it is seen that the signal as sampled at coastal stations contains a significant amount of local noise. Since such noise may be present, the

"smoothed" tide signal resulting from the least squares adjustment done on the ALS survey observations may be more accurate since most of the observations were made away from the coast. Also, as the spatial resolution of the tidal zoning becomes finer, the accuracy of the tidal reducers increases.

Based on the evidence presented in this thesis, the determination of tidal reducers for ALS surveys from airborne bathymetric data holds promise for reducing the number of tide gauges needed for an ALS survey.

APPENDIX A

RESULTS OF HARMONIC ANALYSIS

PORT SAN LUIS, CA

MSL	Constit.	R	Zeta	Speed
6.939	1	*1.550	215.41	28.9841
	2	0.487	283.55	30.0000
	3	0.363	299.89	28.4397
	4	1.292	82.68	15.0411
	5	0.002	308.74	57.9682
	6	0.857	18.89	13.9430
	7	0.005	125.24	86.9523
	8	0.003	193.85	44.0252
	9	0.002	160.25	60.0000
	10	0.003	53.54	57.4238
	11	0.066	12.63	28.5126
	12	0.003	87.15	90.0000
	13	0.049	80.61	27.9682
	14	0.043	23.92	27.8954
	15	0.073	339.47	16.1391
	16	0.011	242.58	29.4556
	17	0.023	34.84	15.0000
	18	0.038	164.68	14.4967
	19	0.033	346.61	15.5854
	20	0.025	17.38	0.5444
	21	0.147	107.16	0.0821
	22	0.126	229.15	0.0411
	23	0.015	27.11	1.0159
	24	0.037	50.41	1.0980
	25	0.029	194.21	13.4715
	26	0.157	117.55	13.9397
	27	0.025	267.76	29.9589
	28	0.003	127.63	30.0411
	29	0.016	221.63	12.8543
	30	0.365	101.81	14.9589
	31	0.009	172.80	31.0159
	32	0.009	243.57	43.4762
	33	0.031	316.19	29.5285
	34	0.003	310.53	42.9271
	35	0.185	72.67	30.0821
	36	0.004	55.26	115.9364
	37	0.005	77.42	58.9841

MONTEREY, CA

MSL	Constit.	R	Zeta	Speed
6.063	1	1.551	228.55	28.9841
	2	0.423	300.30	30.0000
	3	0.361	310.94	28.4397
	4	1.330	88.10	15.0411
	5	0.005	359.86	57.9682
	6	0.832	23.58	13.9430
	7	0.002	342.89	86.9523
	8	0.003	53.51	44.0252
	9	0.001	349.52	60.0000
	10	0.006	77.90	57.4238
	11	0.063	26.44	28.5126
	12	0.003	125.55	90.0000
	13	0.040	92.47	27.9682
	14	0.041	33.24	27.8954
	15	0.076	344.60	16.1391
	16	0.004	231.85	29.4556
	17	0.040	43.37	15.0000
	18	0.088	173.35	14.4967
	19	0.031	353.06	15.5854
	20	0.040	26.52	0.5444
	21	0.135	102.45	0.0821
	22	0.104	258.57	0.0411
	23	0.032	11.43	1.0159
	24	0.051	45.97	1.0980
	25	0.032	204.33	13.4715
	26	0.164	123.36	13.3987
	27	0.022	290.08	29.9589
	28	0.006	99.75	30.0411
	29	0.019	231.72	12.8543
	30	0.374	106.86	14.9589
	31	0.004	229.61	31.0159
	32	0.007	259.89	43.4762
	33	0.037	332.40	29.5285
	34	0.004	1.82	42.9271
	35	0.158	85.87	30.0821
	36	0.002	195.77	115.9364
	37	0.002	79.53	58.9841

LIST OF REFERENCES

Billard, B., "Assessment of Various Configurations for Locating the Mean Sea Surface Reference in Laser Hydrography," International Hydrographic Review, v. LXVI(1), pp. 93-113, January 1989.

Billard, B., "Estimation of Mean Sea Surface Reference in the WRELADS Airborne Depth Sounder," Applied Optics, v. 25, No. 13, pp. 2067-2073, 1 July 1986.

Brown, R.D., "M2 Ocean Tide at Cobb Seamount from Seasat Altimeter Data," Journal of Geophysical Research, v. 88, No. C3, pp. 1637-1646, Feb. 28, 1983.

Carrara, G., and Vanicek, P., "The Use of Sea Level Tide Gauge Observations in Geodesy," Lighthouse, Ed. No. 31, pp. 13-20, May 1985.

Casey, M.M., and Vosburgh, J., "Airborne Hydrographic Surveying in the Canadian Arctic," International Hydrographic Review, v. LXIV(1), pp. 111-121, 1987.

Casey, M.M., and Vosburgh, J., "Chartmaking with Larsen," The Canadian Surveyor, v. 40, No. 3, pp. 251-260, Autumn 1986.

Caviness, R., "Airborne Bathymetric Survey (ABS) System Operational Scenario: Synopsis," draft internal document at U.S. Naval Oceanographic Office, 1989.

Clarke, A.J., and Battisti, D.S., "The Effect of Continental Shelves on Tides," Deep Sea Research, v. 28A, No. 7, pp. 665-682, 1981.

Dickman, S.R., "Theoretical Investigation of the Oceanic Inverted Barometer Response," Journal of Geophysical Research, v. 93, No. B12, pp. 14,941-14,946, 10 December 1988.

Duxbury, A.C., and Duxbury, A.B., An Introduction to the World's Oceans, Addison-Wesley Publishing Co., 1984.

Enabnit, D.B., and Nield, Cdr. V.K., USN, "Airborne Laser Hydrography," International Hydrographic Review, v. LVII(2), pp. 93-97.

Guenther, G., NOAA Charting Research and Development Laboratory Nautical Charting Division National Ocean Service, NOAA, Rockville, Maryland, 20852, Subject: Estimated Accuracy

Possible for Mean Water Surface Measurement with Airborne Laser, August 1989.

Hickman, G.D., and others, "The Airborne Bathymetric Survey System," Marine Technology Society Journal, v. 20, No. 2, pp. 5-13, 1986.

Hoge, F.E., Swift, R.N., and Frederick, E.B., "Water Depth Measurement Using an Airborne Pulsed Neon Laser System," Applied Optics, v. 19, No. 6, pp. 871-883, 15 March 1980.

Karunaratne, D.A., "An Improved Method for Smoothing and Interpolating Hourly Sea Level Data," International Hydrographic Review, v. LVII(1), pp. 135-148, January 1980.

Kleusberg, A., and others, GPS Relative Positioning Techniques for Moving Platforms, Proc. 4th Intern. Geod. Symp. Sat. Pos., Austin, TX, pp. 1299-1310, 1986.

Krabill, W.B., and Martin, C.F., "Aircraft Positioning Using Global Positioning System Carrier Phase Data," Navigation: Journal of the Institute of Navigation, v. 34, No. 1, pp. 1-22, Spring 1987.

Leblond, P.H. and Mysak, L.A., Waves in the Ocean, 2nd ed., Elsevier Scientific Publishing Company, 1980.

Malone, A.K., Casey, M.J., and Monahan, D., "Scanning LIDAR Bathymeter (1) Deployment Strategies," Lighthouse, ed. No. 27, pp. 2-6, 1983.

Mader, G.L., and Lucas, J.R., "Dynamic Positioning with GPS," Proceedings: 3rd Biennial National Ocean Service International Hydrographic Conference, pp. 17-23, 12-15 April 1988.

Marmer, H.A., U.S. Department of Commerce, Coast and Geodetic Survey, Tidal Datum Planes, Spec. Pub. No, 135, pp. 45-49, Government Printing Office, Washington, DC, 1951.

Munk, W., Snodgrass, F., and Wimbush, M., "Tides Off-Shore: Transition from California Coastal to Deep-Sea Waters," Geophysical Fluid Dynamics, v. 1, pp. 161-235, 1970.

Penny, M.F., and others, "Airborne Laser Hydrography in Australia," Applied Optics, v. 25, No. 13, pp. 2046-2058.

Schureman, P., U.S. Department of Commerce, Coast and Geodetic Survey, Manual of Harmonic Analysis and Prediction of Tides, Special Publication No. 98, Government Printing Office, 1971.

Unknown Author, Hydrographic Department Admiralty, Admiralty Tidal Handbook No. 2, N.P.122(2), Datums for Hydrographic Surveys (and other related subjects), pp. 25-26, Crown, 1975.

Uotila, U.A., Notes on Adjustment Computations, Part I, Department of Geodetic Science and Surveying, Ohio State University, 1986.

Wells, D.E., and others, Guide to GPS Position, Canadian GPS Associates, 1986.

INITIAL DISTRIBUTION LIST

		No. Copies
1.	Defense Technical Information Center Cameron Station Alexandria, VA 22304-6145	2
2.	Library, Code 0142 Naval Postgraduate School Monterey, CA 93943-5002	2
3.	Kurt Schnebele, Code 68Sn Department of Oceanography Naval Postgraduate School Monterey, CA 93943-5000	2
4.	Chairman, Code 68Mr Department of Oceanography Naval Postgraduate School Monterey, CA 93943-5000	1
5.	Jeff Nystuen, Code 68Ny Department of Oceanography Naval Postgraduate School Monterey, CA 93943-5000	1
6.	Timothy Tisch SMC Box #2758 Naval Postgraduate School Monterey, CA 93943-5000	1
7.	Rebecca Caviness, Code HST United States Naval Oceanographic Office Stennis Space Center, MS 39522-5001	1
8.	Robert Bullard, Code HSS United States Naval Oceanographic Office Stennis Space Center, MS 39522-5001	1
9.	George Walker, Code H United States Naval Oceanographic Office Stennis Space Center, MS 39522-5001	1

10. Gary Guenther 1
National Oceanic and Atmospheric Administration
Charting Research and Development Lab
Nautical Charting Division
National Ocean Service, NOAA
Rockville, MD 20852

11. Steve Gill 1
N/OMA 122
National Oceanic and Atmospheric Administration
Rockville, MD 20852

12. John Hannah 1
Department of Survey and Land Information
P.O. Box 170
Wellington, New Zealand

13. Leslie Rosenfeld 1
Monterey Bay Aquarium Research Institute
1600 Central Avenue
Pacific Grove, CA 93950

14. Director Naval Oceanography Division 1
Naval Observatory
34th and Massachusetts Avenue NW
Washington, DC 20390

15. Commander 1
Naval Oceanography Command
Stennis Space Center
Bay Saint Louis, MS 39522

16. Commanding Officer 1
Naval Oceanographic Office
Stennis Space Center
Bay Saint Louis, MS 39522

17. Commanding Officer 1
Naval Ocean Research and Development Activity
Stennis Space Center
Bay Saint Louis, MS 39522

18. Chairman, Oceanography Department 1
United States Naval Academy
Annapolis, MD 21402

19. Chief of Naval Research 1
800 N. Quincy Street
Arlington, VA 22217

20. Director, Code PPH 1
Defense Mapping Agency
Building 56, United States Naval Observatory
Washington, DC 20305

21. Director, Code HO 1
Defense Mapping Agency Hydrographic
Topographic Center
6500 Brookes Lane
Washington, DC 20315

22. Director, Code PSD-MC 1
Defense Mapping School
Fort Belvoir, VA 22060

23. Director, Charting and Geodetic 1
Services (N/CG)
National Oceanic and Atmospheric Administration
Rockville, MD 20852

24. Chief, Program Planning, Liaison and 1
Training (NC2)
National Oceanic and Atmospheric Administration
Rockville, MD 20852

25. Chief, Nautical Charting Division (N/CG2) 1
National Oceanic and Atmospheric Administration
Rockville, MD 20852

26. Chief, Hydrographic Surveys Branch (N/CG24) 1
National Oceanic and Atmospheric Administration
Rockville, MD 20852

27. Director, Pacific Marine Center (M/MOP) 1
National Ocean Service, National Oceanic and
Atmospheric Administration
1801 Fairview Avenue East
Seattle, WA 98102

28. Director, Atlantic Marine Center (N/MOA) 1
National Ocean Service, National Oceanic and
Atmospheric Administration
439 W. York Street
Norfolk, VA 23510

29. IHO/FIG International Advisory Board 1
International Hydrographic Bureau
Avenue President J.F. Kennedy
Monte Carlo, Monaco

30. Hydrographer of the Navy 1
Ministry of Defense
Hydrographic Department
Taunton, Somerset
TA129N England

31. Hydrographer, Royal Australian Navy 1
Hydrographic Office
Box 1332 North sydney 2060
New South Wales - Australia

32. Dominion Hydrographer 1
Canadian Hydrographic Service
615 Booth Street
Ottawa, Ontario
Canada KIAOE6

33. Hydrographic Service 1
Athens BST 902
Greece

34. Commanding Officer 1
NOAA SHIP FERREL
Atlantic Marine Center, National Oceanic and
Atmospheric Administration
439 West York Street
Norfolk, VA 23510

35. Chief, Hydrographic Surveys Branch 1
Atlantic Marine Center, National Oceanic and
Atmospheric Administration
439 West York Street
Norfolk, VA 23510

36. Ken Welker, Code HT 1
United States Naval Oceanographic Office
Stennis Space Center
Bay Saint Louis, MS 39522-5001

Thesis
W4143
c.1

Welker
Determination of tide heights from airborne bathymetric data.